QCD corrections and nonstandard three vector boson couplings in W^+W^- production at hadron colliders

U. Baur

Department of Physics, State University of New York at Buffalo, Buffalo, New York 14260

T. Han and J. Ohnemus

Department of Physics, University of California, Davis, California 95616
(Received 18 July 1995)

The process $p\overset{(-)}{p} \to W^+W^- + X \to \ell_1^+\nu_1\ell_2^-\bar\nu_2 + X$ is calculated to $O(\alpha_s)$ for general C- and P-conserving WWV couplings ($V = \gamma, Z$). The prospects for probing the WWV couplings in this reaction are explored. The impact of $O(\alpha_s)$ QCD corrections and various background processes on the observability of nonstandard WWV couplings in W^+W^- production at the Fermilab Tevatron and the CERN Large Hadron Collider (LHC) is discussed in detail. The transverse momentum distribution of the charged lepton pair is found to be particularly sensitive to both anomalous couplings and QCD corrections. Sensitivity limits for anomalous WWV couplings are derived at next-to-leading-order for the Fermilab Tevatron and LHC center-of-mass energies, and are compared to the bounds which can be achieved in other processes. Unless a jet veto or a cut on the total transverse momentum of the hadrons in the event is imposed, the $O(\alpha_s)$ QCD corrections and the background from top quark production decrease the sensitivity of $p\overset{(-)}{p} \to W^+W^- + X \to \ell_1^+\nu_1\ell_2^-\bar\nu_2 + X$ to anomalous WWV couplings by a factor 2 to 5.

PACS number(s): 12.38.Bx, 14.70.Fm

I. INTRODUCTION

The electroweak standard model (SM) based on an $SU(2) \otimes U(1)$ gauge theory has been remarkably successful in describing contemporary high energy physics experiments; however, the three vector boson couplings predicted by this non-Abelian gauge theory remain largely untested. A precise measurement of these couplings will soon be possible in W pair production at the CERN e^+e^- collider LEP II [1,2]. With the large data samples collected in the present Fermilab Tevatron collider run, and plans for further upgrades in luminosity [3], the production of W^+W^- pairs at hadron colliders provides an alternative and increasingly attractive opportunity to study the $WW\gamma$ and WWZ vertices [4–8]. Recently, the Collider Detector at Fermilab (CDF) and D0 Collaborations reported first measurements of the WWV couplings ($V = \gamma, Z$) in W^+W^- production at the Tevatron from the data collected in the 1992–1993 run. CDF used the reaction $p\bar{p} \to W^+W^- \to \ell^\pm\nu jj$, $\ell = e, \mu$ [9] to derive limits on anomalous three vector boson couplings, whereas D0 analyzed the dilepton channels, $p\bar{p} \to W^+W^- \to \ell_1^+\nu_1\ell_2^-\bar\nu_2$, $\ell_{1,2} = e, \mu$ [10]. In the SM, the WWV vertices are completely fixed by the $SU(2) \otimes U(1)$ gauge structure of the electroweak sector, thus a measurement of these vertices provides a stringent test of the SM.

In contrast with low energy data and high precision measurements at the Z peak, collider experiments offer the possibility of a direct, and essentially model-independent, determination of the three vector boson vertices. Previous theoretical studies on probing the WWV vertices via hadronic W^+W^- production have been based on leading-order (LO) calculations [4–8]. The prospects for extracting information on anomalous WWV couplings from decay modes where one of the W bosons decays into leptons and the second into hadrons, $W^+W^- \to \ell^\pm\nu jj$, have been discussed in Ref. [7]. A detailed discussion of the purely leptonic channels, $W^+W^- \to \ell_1^+\nu_1\ell_2^-\bar\nu_2$, has not yet appeared in the literature. In general, the inclusion of anomalous couplings at the $WW\gamma$ and WWZ vertices yields enhancements in the W^+W^- cross section, especially at large values of the W boson transverse momentum, $p_T(W)$, and at large values of the W^+W^- invariant mass, M_{WW}. Next-to-leading-order (NLO) calculations of hadronic W^+W^- production have shown that the $O(\alpha_s)$ corrections are large in precisely these same regions [11,12]. It is thus vital to include the $O(\alpha_s)$ corrections when using hadronic W^+W^- production to probe the $WW\gamma$ and WWZ vertices.

In this paper, we calculate hadronic W^+W^- production to $O(\alpha_s)$, including the most general, C- and P-conserving, anomalous $WW\gamma$ and WWZ couplings, and discuss in detail the purely leptonic decay modes, $W^+W^- \to \ell_1^+\nu_1\ell_2^-\bar\nu_2$. Decay channels where one or both of the W bosons decay into hadrons are not considered here. Presently, experiments only place an upper limit on the cross section for W^+W^- production in hadronic collisions [9,10]. With CDF and D0 rapidly approaching their goal of an integrated luminosity of 100 pb^{-1} in the current Tevatron run, this situation is expected to change soon [13]. In the Main Injector Era, integrated luminosities of order 1 fb^{-1} are envisioned [3,14], and a sufficient number of events should be available to

commence a detailed investigation of the WWV vertices in the $W^+W^- \to \ell_1^+ \nu_1 \ell_2^- \bar{\nu}_2$ channel, provided that the background can be controlled. The prospects for a precise measurement of the WWV couplings in this channel would further improve if a significant upgrade in luminosity beyond the goal of the Main Injector could be realized. With recent advances in accelerator technology [14], Tevatron collider luminosities of order 10^{33} cm^{-2} s^{-1} may become reality within the next few years, resulting in integrated luminosities of up to 10 fb^{-1} per year (a luminosity upgraded Tevatron will henceforth be denoted by TeV*). At the CERN Large Hadron Collider [(LHC), pp collisions at $\sqrt{s} = 14$ TeV [15]], the $t\bar{t}$ background needs to be reduced by at least one order of magnitude in order to utilize the potential of the process $pp \to W^+W^- + X$ to constrain anomalous gauge boson couplings.

Compared to other processes which are sensitive to the structure of the WWV vertices, W^+W^- production has an important advantage. Terms proportional to the anomalous coupling $\Delta\kappa_V$ in the amplitude [see Eq. (1) for a definition of the anomalous couplings] grow like $\hat{s}/M_W^2$ [1], where $\hat{s}$ is the parton center-of-mass energy squared, whereas these terms increase only like $\sqrt{\hat{s}}/M_W$ in $W^\pm\gamma$ and $W^\pm Z$ production. One therefore expects that W^+W^- production is considerably more sensitive to $\Delta\kappa_V$ than $p\overset{(-)}{p} \to W^\pm\gamma$, $W^\pm Z$.

To perform our calculation, we use the Monte Carlo method for NLO calculations described in Ref. [16]. The leptonic decays of the W bosons are included using the narrow width approximation. With the Monte Carlo method, it is easy to calculate a variety of observables simultaneously and to implement experimental acceptance cuts in the calculation. It is also possible to compute the $O(\alpha_s)$ QCD corrections for exclusive channels, e.g., $p\overset{(-)}{p} \to W^+W^- + 0$ jet. Apart from anomalous contributions to the $WW\gamma$ and WWZ vertices, the SM is assumed to be valid in the calculation. In particular, the couplings of the weak bosons to quarks and leptons are assumed to have their SM values. Section II briefly summarizes the technical details of our calculation.

The results of our numerical simulations are presented in Sec. III. In contrast to the SM contributions to the $q\bar{q} \to W^+W^-$ helicity amplitudes, terms associated with nonstandard WWV couplings grow with energy. Distributions which reflect the high energy behavior of the helicity amplitudes, such as the invariant mass distribution, the transverse momentum spectrum of the charged lepton pair, or the transverse momentum distribution of the individual leptons, are therefore very sensitive to anomalous WWV couplings. We identify the transverse momentum distribution of the charged lepton pair, $d\sigma/dp_T(\ell_1^+\ell_2^-)$, as the distribution which, at leading-order (LO), is most sensitive to the WWV couplings, and discuss the impact of QCD corrections on this and other distributions. In contrast to other distributions, the LO $p_T(\ell_1^+\ell_2^-)$ distribution is not only sensitive to the high energy behavior of the W^+W^- production amplitudes, but also provides indirect information on the helicities of the W bosons, which are strongly correlated in W pair production in the SM [1,5,17]. Since anomalous WWV

couplings modify both the high energy behavior of the amplitudes and the correlations between the W helicities, $d\sigma/dp_T(\ell_1^+\ell_2^-)$ is particularly sensitive to these couplings. We also investigate in detail the background processes contributing to $p\overset{(-)}{p} \to W^+W^- + X \to \ell_1^+\nu_1\ell_2^-\bar{\nu}_2 + X$, in particular, the $t\bar{t}$ background. Both the QCD corrections and the top quark background are found to be large. They change the shape of the $p_T(\ell_1^+\ell_2^-)$ distribution, and reduce the sensitivity to anomalous WWV couplings significantly.

In Sec. III, we also show that the size of the QCD corrections and the $t\bar{t}$ background can be greatly reduced, and a significant fraction of the sensitivity lost can be regained, if either a jet veto, or a cut on the transverse momentum of the hadrons in the event, is imposed. Finally, we derive sensitivity limits for anomalous WWV couplings for various integrated luminosities at the Tevatron and LHC, and compare them with those which can be achieved in $W^\pm\gamma$ and $W^\pm Z$ production, and in $e^+e^- \to W^+W^-$. Our conclusions are given in Sec. IV.

II. CALCULATIONAL TOOLS

The calculation presented here generalizes the results of Ref. [18] to include arbitrary C- and P-conserving $WW\gamma$ and WWZ couplings, and employs a combination of analytic and Monte Carlo integration techniques. Details of the method can be found in Ref. [16]. The calculation is performed using the narrow width approximation for the leptonically decaying W bosons. In this approximation difficulties in implementing finite W width effects while maintaining electromagnetic gauge invariance [19] are automatically avoided, and it is straightforward to extend the NLO calculation of W^+W^- production for on-shell W bosons to include the leptonic decays of the W bosons. Furthermore, nonresonant Feynman diagrams, such as $u\bar{u} \to Z^* \to e^+e^-Z$ followed by $Z \to \nu\bar{\nu}$, contribute negligibly in this limit and can be ignored. Finite W width effects and nonresonant diagrams play an important role in the W pair threshold region. For the cuts we impose (see Sec. III B), the threshold region contributes negligibly to the cross section.

A. Summary of $O(\alpha_s)$ W^+W^- production including leptonic W decays

The NLO calculation of W^+W^- production includes contributions from the square of the Born graphs, the interference between the Born graphs and the virtual one-loop diagrams, and the square of the real emission graphs. The basic idea of the method employed here is to isolate the soft and collinear singularities associated with the real emission subprocesses by partitioning phase space into soft, collinear, and finite regions. This is done by introducing theoretical soft and collinear cutoff parameters, δ_s and δ_c. Using dimensional regularization [20], the soft and collinear singularities are exposed as poles

in ϵ (the number of space-time dimensions is $N = 4 - 2\epsilon$ with ϵ a small number). The infrared singularities from the soft and virtual contributions are then explicitly canceled while the collinear singularities are factorized and absorbed into the definition of the parton distribution functions. The remaining contributions are finite and can be evaluated in four dimensions. The Monte Carlo program thus generates n-body (for the Born and virtual contributions) and $(n+1)$-body (for the real emission contributions) final state events. The n- and $(n + 1)$-body contributions both depend on the cutoff parameters δ_s and δ_c, however, when these contributions are added together to form a suitably inclusive observable, all dependence on the cutoff parameters cancels. The numerical results presented in this paper are insensitive to variations of the cutoff parameters.

Except for the virtual contribution, the $O(\alpha_s)$ corrections are all proportional to the Born cross section. It is easy to incorporate the leptonic W decays into those terms which are proportional to the Born cross section; one simply replaces $d\hat{\sigma}^{\mathrm{Born}}(q\bar{q} \to W^+W^-)$ with $d\hat{\sigma}^{\mathrm{Born}}(q\bar{q} \to W^+W^- \to \ell_1^+\nu_1\ell_2^-\bar{\nu}_2)$ in the relevant formulas. When working at the amplitude level, the W boson decays are trivial to implement; the W boson polarization vectors, $\epsilon_\mu(k)$, are simply replaced by the corresponding $W \to \ell\nu$ decay currents, $J_\mu(k)$, in the amplitude. Details of the amplitude level calculations for the Born and real emission subprocesses can be found in Ref. [21].

The only term in which it is more difficult to incorporate the W boson decays is the virtual contribution. Rather than undertake the nontrivial task of recalculating the virtual correction term for the case of leptonically decaying W bosons, we have instead opted to use the virtual correction for real on-shell W bosons which we subsequently decay ignoring spin correlations. When spin correlations are ignored, the spin summed squared matrix element factorizes into separate production and decay squared matrix elements. Neglecting spin correlations slightly modifies the shapes of the angular distributions of the final state leptons, but does not alter the total cross section as long as no angular cuts (e.g., rapidity cuts) are imposed on the final state leptons. For realistic rapidity cuts, cross sections are changed by typically 10% when spin correlations are neglected. Since the size of the finite virtual correction is less than $\sim 10\%$ the size of the Born cross section, the overall effect of neglecting the spin correlations in the finite virtual correction is expected to be negligible compared to the combined 10–20% uncertainty from the parton distribution functions, the choice of the factorization scale Q^2, and higher order QCD corrections.

B. Incorporation of anomalous $WW\gamma$ and WWZ couplings

The $WW\gamma$ and WWZ vertices are uniquely determined in the SM by $SU(2) \otimes U(1)$ gauge invariance. In W^+W^- production, the W bosons couple to essentially massless fermions, which ensures that effectively $\partial_\mu W^\mu = 0$. This condition, together with Lorentz invariance and conservation of C and P, allows six free parameters, g_1^V, κ_V, and λ_V in the WWV vertices ($V = \gamma, Z$). The most general WWV vertex, which is Lorentz, C, and P invariant, is described by the effective Lagrangian [1]

$$\mathcal{L}_{WWV} = -ig_{WWV}\left[g_1^V\left(W_{\mu\nu}^\dagger W^\mu V^\nu - W_\mu^\dagger V_\nu W^{\mu\nu}\right) + \kappa_V W_\mu^\dagger W_\nu V^{\mu\nu} + \frac{\lambda_V}{M_W^2}W_{\lambda\mu}^\dagger W_\nu^\mu V^{\nu\lambda}\right], \quad (1)$$

where g_{WWV} is the WWV coupling strength ($g_{WW\gamma} = e$ and $g_{WWZ} = e\cot\theta_W$, where e is the electric charge of the proton and θ_W is the weak mixing angle), W^μ is the W^- field, V^μ denotes the Z boson or photon field, $W_{\mu\nu} = \partial_\mu W_\nu - \partial_\nu W_\mu$, and $V_{\mu\nu} = \partial_\mu V_\nu - \partial_\nu V_\mu$. At tree level in the SM, $g_1^V = 1$, $\kappa_V = 1$, and $\lambda_V = 0$. All higher dimensional operators are obtained by replacing X^μ with $(\partial^2)^m X^\mu$ ($X = W, Z, \gamma$), where m is an arbitrary positive integer, in the terms proportional to $\Delta g_1^V = g_1^V - 1$, $\Delta\kappa_V = \kappa_V - 1$, and λ_V. These operators form a complete set and can be summed by replacing Δg_1^V, $\Delta\kappa_V$, and λ_V with momentum-dependent form factors. All details are contained in the specific functional form of the form factor and its scale Λ_{FF}. For the $WW\gamma$ vertex, electromagnetic gauge invariance requires that for on-shell photons $\Delta g_1^\gamma = 0$. Hence, the corresponding form factor must be proportional to some positive power of the square of the photon momentum, q_γ^2. Δg_1^γ therefore is of $O(q_\gamma^2/\Lambda_{\mathrm{FF}}^2)$ and terms proportional to Δg_1^γ in the helicity amplitudes are suppressed for momentum transfer smaller than the form factor scale. To simplify our discussion somewhat, we assume in the following that $\Delta g_1^\gamma = 0$. The high energy behavior of the form factors Δg_1^Z, $\Delta\kappa_V$, and λ_V will be discussed in more detail later in this section.

Following the standard notation of Ref. [1], we have chosen, without loss of generality, the W boson mass M_W as the energy scale in the denominator of the term proportional to λ_V in Eq. (1). If a different mass scale M had been used, then all of our subsequent results could be obtained by scaling λ_V by a factor $\mathtt{M}^2/M_W^2$.

At present, the WWV coupling constants are only weakly constrained experimentally (for a recent summary and discussion see Ref. [22]). From a search performed in the channels $p\bar{p} \to W^+W^-$, $W^\pm Z \to \ell^\pm\nu jj$, and $p\bar{p} \to WZ \to jj\ell^+\ell^-$ ($\ell = e, \mu$) at large dijet transverse momenta, the CDF Collaboration obtains, for $\Delta\kappa_\gamma = \Delta\kappa_Z$ and $\lambda_\gamma = \lambda_Z$ [9],

$$-1.1 < \Delta\kappa_V < 1.3 \quad (\text{for } \lambda_V = \Delta g_1^V = 0),$$
$$ \tag{2}$$
$$-0.8 < \lambda_V < 0.8 \quad (\text{for } \Delta\kappa_V = \Delta g_1^V = 0),$$

at the 95% confidence level (C.L.). Assuming that all other couplings take their SM values, CDF also obtains a 95% C.L. limit on Δg_1^Z of

$$-1.2 < \Delta g_1^Z < 1.2. \quad (3)$$

Slightly worse (better) limits on $\Delta\kappa_\gamma$ (λ_γ) are obtained from $W^\pm\gamma$ production at the Tevatron [23,24]. From a comparison of their 95% C.L. upper limit on the total $W^+W^- \to \ell_1^+\nu_1\ell_2^-\bar\nu_2$ cross section with the SM prediction, the D0 Collaboration finds, for $\Delta\kappa_\gamma = \Delta\kappa_Z$ and $\lambda_\gamma = \lambda_Z$ [10],

$$-2.6 < \Delta\kappa_V < 2.8 \quad (\text{for } \lambda_V = \Delta g_1^V = 0),$$

$$(4)$$

$$-2.2 < \lambda_V < 2.2 \quad (\text{for } \Delta\kappa_V = \Delta g_1^V = 0).$$

To derive these limits, CDF (D0) assumed a dipole form factor with scale $\Lambda_{\rm FF} = 1.0$ TeV (0.9 TeV) [see below], however, the experimental bounds are quite insensitive to the value of $\Lambda_{\rm FF}$.

Although bounds on the WWV couplings can also be extracted from low energy data and oblique corrections to the four-fermion S-matrix elements, there are ambiguities and model dependencies in the results [22,25–28]. From loop contributions to $(g-2)_\mu$ [29], $b \to s\gamma$ [30,31], rare meson decays such as $K_L \to \mu^+\mu^-$ [32] or $B \to K^{(*)}\mu^+\mu^-$ [33], ϵ'/ϵ [34], and the $Z \to b\bar b$ width [35], one estimates limits for the nonstandard WWV couplings of $\sim$ 1–10. No rigorous bounds can be obtained from oblique corrections, which combine [36,37] information from recent LEP/or SLAC Linear Collider Large Detector (SLD) data, neutrino scattering experiments, atomic parity violation, μ decay, and the W-mass measurement at hadron colliders, if correlations between different contributions to the anomalous couplings are fully taken into account. Even without serious cancellations among various one-loop contributions, anomalous WWV couplings of order 1 are still allowed by present data [22,27]. In contrast, invoking a "naturalness" argument based on chiral perturbation theory [38,39], one expects deviations from the SM of $\sim 10^{-2}$ or less for g_1^V, κ_V, and λ_V.

If C- or P-violating couplings are allowed, four additional free parameters, g_4^V, g_5^V, $\tilde\kappa_V$ and $\tilde\lambda_V$ appear in the effective WWV Lagrangian [1]. For simplicity, these couplings are not considered in this paper.

The Feynman rule for the WWV vertex factor corresponding to the Lagrangian in Eq. (1) is

$$-i\, g_{WWV}\, \Gamma_{\beta\mu\nu}(k, k_1, k_2)$$

$$= -i\, g_{WWV}\, [\Gamma^{\rm SM}_{\beta\mu\nu}(k, k_1, k_2) + \Gamma^{\rm NSM}_{\beta\mu\nu}(k, k_1, k_2)], \quad (5)$$

where the labeling conventions for the four-momenta and Lorentz indices are defined by Fig. 1, and the factors $\Gamma^{\rm SM}$ and $\Gamma^{\rm NSM}$ are the SM and nonstandard model vertex factors:

$$\Gamma^{\rm SM}_{\beta\mu\nu}(k, k_1, k_2) = (k_1 - k_2)_\beta\, g_{\nu\mu} + 2\, k_\mu\, g_{\beta\nu} - 2\, k_\nu\, g_{\beta\mu},$$
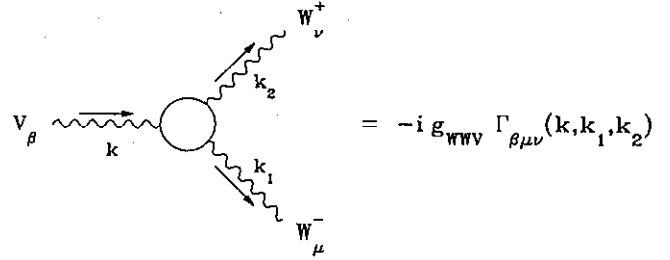
$$(6)$$

FIG. 1. Feynman rule for the general WWV ($V = \gamma, Z$) vertex. The factor g_{WWV} is the vertex coupling strength: $g_{WW\gamma} = e$ and $g_{WWZ} = e\cot\theta_W$. The vertex function $\Gamma_{\beta\mu\nu}(k, k_1, k_2)$ is given in Eq. (5).

$$\Gamma^{\rm NSM}_{\beta\mu\nu}(k, k_1, k_2) = \left(\Delta g_1^V + \lambda_V\, \frac{k^2}{2M_W^2}\right)(k_1 - k_2)_\beta\, g_{\nu\mu}$$

$$- \frac{\lambda_V}{M_W^2}\, (k_1 - k_2)_\beta\, k_\nu\, k_\mu$$

$$+ (\Delta g_1^V + \Delta\kappa_V + \lambda_V)\, k_\mu\, g_{\beta\nu}$$

$$- (\Delta g_1^V + \Delta\kappa_V + \lambda_V)\, k_\nu\, g_{\beta\mu}. \quad (7)$$

The nonstandard model vertex factor is written here in terms of $\Delta g_1^V = g_1^V - 1$, $\Delta\kappa_V = \kappa_V - 1$, and λ_V, which all vanish in the SM.

It is straightforward to include the nonstandard model couplings in the amplitude level calculations. The $q\bar q \to W^+W^-$ virtual correction with the modified vertex factor of Eq. (5) has been computed using the computer algebra program FORM [40]; however, the resulting expression is too lengthy to present here. The nonstandard $WW\gamma$ and WWZ couplings of Eq. (1) do not destroy the renormalizability of QCD. Thus the infrared singularities from the soft and virtual contributions are explicitly canceled, and the collinear singularities are factorized and absorbed into the definition of the parton distribution functions, exactly as in the SM case.

The anomalous couplings cannot be simply inserted into the vertex factor as constants because this would violate S-matrix unitarity. Tree-level unitarity uniquely restricts the WWV couplings to their SM gauge theory values at asymptotically high energies [41]. This implies that any deviation of Δg_1^V, $\Delta\kappa_V$, or λ_V from the SM expectation has to be described by a form factor $\Delta g_1^V(M_{WW}^2, p_{W^+}^2, p_{W^-}^2)$, $\Delta\kappa_V(M_{WW}^2, p_{W^+}^2, p_{W^-}^2)$, or $\lambda_V(M_{WW}^2, p_{W^+}^2, p_{W^-}^2)$ which vanishes when either the square of the W^+W^- invariant mass, M_{WW}^2, or the square of the four-momentum of a final state W boson ($p_{W^+}^2$ or $p_{W^-}^2$) becomes large. In W^+W^- production, $p_W^2 \approx M_W^2$ even when the finite W width is taken into account. However, large values of M_{WW}^2 will be probed at future hadron colliders like the LHC and the M_{WW}^2 dependence of the anomalous couplings has to be included in order to avoid unphysical results which would violate unitarity. Consequently, the anomalous couplings (denoted generically by a, $a = \Delta g_1^V, \Delta\kappa_V, \lambda_V$) are introduced via form factors [42]. The functional behavior of the form factors depends on the details of the underlying

new physics. Effective Lagrangian techniques are of little help here because the low energy expansion which leads to the effective Lagrangian exactly breaks down where the form factor effects become important. Therefore, ad hoc assumptions have to be made. Here, we assume a behavior similar to the nucleon form factor

$$a(M_{WW}^2, p_{W^+}^2 = M_W^2, p_{W^-}^2 = M_W^2)$$

$$= \frac{a^0}{(1 + M_{WW}^2/\Lambda_{FF}^2)^n} , \quad (8)$$

where a^0 is the form factor value at low energies and Λ_{FF} represents the scale at which new physics becomes important in the weak boson sector. In order to guarantee unitarity, it is necessary to have $n > 1$. For the numerical results presented here, we use a dipole form factor ($n = 2$) with a scale $\Lambda_{FF} = 1$ TeV, unless explicitly stated otherwise. The exponent $n = 2$ is chosen in order to suppress W^+W^- production at energies $\sqrt{\hat{s}} > \Lambda_{FF} \gg M_W$, where novel phenomena like resonance or multiple weak boson production are expected to become important.

Form factors are usually not introduced if an ansatz based on chiral perturbation theory is used. In the framework of chiral perturbation theory, the effective Lagrangian describing the anomalous vector boson self-interactions breaks down at center-of-mass energies above a few TeV [38,39] (typically $4\pi v \sim 3$ TeV, where $v \approx 246$ GeV is the Higgs field vacuum expectation value). Consequently, one has to limit the center-of-mass energies to values sufficiently below $4\pi v$ in this approach.

The electroweak symmetry can either be realized in a linear [22,27] or nonlinear way [22,26,28]. If the SU(2) ⊗ U(1) symmetry is realized linearly, and only dimension-6 operators are considered, there are 11 independent, SU(2) ⊗ U(1)-invariant, dimension-6 operators [43]. Three of these operators give rise to nonstandard WWV couplings [27]. In this scenario, both anomalous $WW\gamma$ and WWZ couplings are simultaneously nonzero. Assuming, for simplicity, that the coefficients of the two operators which generate nonzero values of $\Delta\kappa_\gamma$ and $\Delta\kappa_Z$ are equal, only two independent anomalous couplings remain [this scenario is known as the Hagiwara-Ishihara-Szalapski-Zeppenfeld (HISZ) scenario (see Ref. [27])]. Choosing, for example, $\Delta\kappa_\gamma$ and λ_γ as independent parameters, the WWZ couplings are then given by

$$\Delta g_1^Z = \frac{1}{2\cos^2\theta_W} \Delta\kappa_\gamma, \quad (9)$$

$$\Delta\kappa_Z = \frac{1}{2}\left(1 - \tan^2\theta_W\right)\Delta\kappa_\gamma, \quad (10)$$

$$\lambda_Z = \lambda_\gamma. \quad (11)$$

In Secs. III E and III G we shall use the HISZ scenario, defined by these equations, as a simple and illustrative example of a model where both $WW\gamma$ and WWZ couplings simultaneously deviate from their SM values. Equations (9)–(11) are modified when operators of dimension 8 or higher are incorporated [27], which may in-

troduce large corrections [37]. Different relations are obtained by invoking global symmetry arguments, or by fine tuning anomalous WWV couplings such that the most serious unitarity-violating contributions to the tree-level vector boson scattering amplitudes are avoided [44].

III. PHENOMENOLOGICAL RESULTS

We shall now discuss the phenomenological implications of $O(\alpha_s)$ QCD corrections in W^+W^- production at the Tevatron ($p\bar{p}$ collisions at $\sqrt{s} = 1.8$ TeV) and the LHC (pp collisions at $\sqrt{s} = 14$ TeV). We first briefly describe the input parameters, cuts, and the finite energy resolution smearing used to simulate detector response. We then explore the sensitivity of the observables in $W^+W^- \to \ell_1^+\nu_1\ell_2^-\bar{\nu}_2$ to anomalous WWV couplings, and discuss in detail the impact of $O(\alpha_s)$ QCD corrections and various background processes on the observability of nonstandard WWV couplings in W^+W^- production at the Tevatron and LHC. To simplify the discussion, we shall concentrate on the channel $W^+W^- \to e^+\nu_e e^-\bar{\nu}_e$. In absence of lepton flavor specific cuts, the cross sections for $W^+W^- \to e^+\nu_e e^-\bar{\nu}_e$ and the other three leptonic channels, $W^+W^- \to \mu^+\nu_\mu\mu^-\bar{\nu}_\mu$, $W^+W^- \to \mu^+\nu_\mu e^-\bar{\nu}_e$, and $W^+W^- \to e^+\nu_e\mu^-\bar{\nu}_\mu$ are equal. Decay modes where one or both charged leptons in the final state originate from $W \to \tau\nu_\tau \to e\nu_e\bar{\nu}_\tau\nu_\tau$ are discussed in Sec. III F. No attempt is made to include the contributions from gluon fusion, $gg \to W^+W^-$, into our calculations, which formally are of $O(\alpha_s^2)$. Gluon fusion contributes less than 1% (15%) to the total W pair cross section at the Tevatron (LHC) [45].

A. Input parameters

The numerical results presented here were obtained using the two-loop expression for α_s. The QCD scale Λ_{QCD} is specified for four flavors of quarks by the choice of the parton distribution functions and is adjusted whenever a heavy quark threshold is crossed so that α_s is a continuous function of Q^2. The heavy quark masses were taken to be $m_b = 5$ GeV and $m_t = 176$ GeV [46,47].

The SM parameters used in the numerical simulations are $M_Z = 91.19$ GeV, $M_W = 80.22$ GeV, $\alpha(M_W) = 1/128$, and $\sin^2\theta_W = 1 - (M_W/M_Z)^2$. These values are consistent with recent measurements at LEP, SLC, the CERN $p\bar{p}$ collider, and the Tevatron [48–50]. The soft and collinear cutoff parameters, discussed in Sec. II A, are fixed to $\delta_s = 10^{-2}$ and $\delta_c = 10^{-3}$. The parton subprocesses have been summed over $u, d, s,$ and c quarks. The W boson leptonic branching ratio is taken to be $B(W \to \ell\nu) = 0.107$ and the total width of the W boson is $\Gamma_W = 2.08$ GeV. Except where otherwise stated, a single scale $Q^2 = M_{WW}^2$, where M_{WW} is the invariant mass of the W^+W^- pair, has been used for the renormalization scale μ^2 and the factorization scale M^2. The NLO numerical results have been calculated in the modified minimal subtraction ($\overline{MS}$) scheme [51]. Our numerical sim-

ulations have been performed using the Martin-Roberts-Stirling (MRS) [52] set A distributions ($\Lambda_4 = 230$ MeV) in the $\overline{\text{MS}}$ scheme.

B. Cuts

The cuts imposed in the numerical simulations are motivated by the finite acceptance of the detectors. The complete set of transverse momentum (p_T) and pseudorapidity (η) cuts can be summarized as follows.

Tevatron	LHC
$p_T(e) > 20$ GeV	$p_T(e) > 25$ GeV
$p\!\!\!/_T > 30$ GeV	$p\!\!\!/_T > 50$ GeV
$|\eta(e)| < 2.5$	$|\eta(e)| < 3.0$

The large missing transverse momentum ($p\!\!\!/_T$) cut has been chosen to reduce potentially dangerous backgrounds from event pileup [53] and processes where particles outside the rapidity range covered by the detector contribute to the missing transverse momentum. These backgrounds are potentially dangerous at the LHC with its large design luminosity of $\mathcal{L} = 10^{34}$ cm^{-2} s^{-1} [15], and also the TeV* under certain conditions. In several of the TeV* scenarios, which are currently under investigation [3,14], the average number of interactions per bunch crossing is similar to that expected at the LHC. Present studies for the LHC [54,55] and extrapolations to Tevatron energies indicate that these backgrounds are under control for the $p\!\!\!/_T$ cuts listed above. The total $W^+W^- \to e^+\nu_e e^-\bar{\nu}_e$, cross section within cuts in the Born approximation at the Tevatron and LHC, is 0.04 pb and 0.15 pb, respectively.

C. Finite energy resolution effects

Uncertainties in the energy measurements of the charged leptons in the detector are simulated in the calculation by Gaussian smearing of the particle four-momentum vector with standard deviation σ. For distributions which require a jet definition, e.g., the $W^+W^- + 1$ jet exclusive cross section, the jet four-momentum vector is also smeared. The standard deviation σ depends on the particle type and the detector. The numerical results presented here for the Tevatron and LHC center-of-mass energies were made using σ values based on the CDF [56] and ATLAS [54] specifications, respectively.

D. Signatures of anomalous WWV couplings and $O(\alpha_s)$ corrections

In contrast to the SM contributions to the $q\bar{q} \to W^+W^-$ helicity amplitudes, terms associated with nonstandard WWV couplings grow with energy. A typical signal for anomalous couplings therefore will be a broad increase in the invariant mass distribution of the W pair at large values of the invariant mass, M_{WW}. Because of the fact that nonstandard WWV couplings only

contribute via s-channel photon and Z exchange, their effects are concentrated in the region of small W rapidities, and the W transverse momentum distribution is particularly sensitive to anomalous couplings. However, if both W bosons decay leptonically, $W^+W^- \to e^+\nu_e e^-\bar{\nu}_e$, the W^+W^- invariant mass and the W transverse momentum cannot be reconstructed since the two neutrinos are not observed.

Alternatively, the invariant mass distribution of the e^+e^- pair, or the electron or positron p_T spectrum can be studied. The differential cross section for $p_T(e)$ in the reaction $p\bar{p} \to W^+W^-+X \to e^+e^-p\!\!\!/_T+X$ at $\sqrt{s} = 1.8$ TeV is shown in Fig. 2. The Born and NLO results are shown in Fig. 2(a) and Fig. 2(b), respectively. Both the e^+ and e^- transverse momenta are histogrammed, each with half the event weight. Results are displayed for the SM and for five sets of anomalous couplings, namely, ($\lambda_\gamma^0 = -0.5$, $\Delta\kappa_\gamma^0 = 0$, SM WWZ couplings), ($\Delta\kappa_\gamma^0 = -0.5$, $\lambda_\gamma^0 = 0$, SM WWZ couplings), ($\lambda_Z^0 = -0.5$, $\Delta g_1^{Z0} = \Delta\kappa_Z^0 = 0$, SM $WW\gamma$ couplings), ($\Delta\kappa_Z^0 = -0.5$, $\Delta g_1^{Z0} = \lambda_Z^0 = 0$, SM $WW\gamma$ couplings), and ($\Delta g_1^{Z0} = -1$, $\Delta\kappa_Z^0 = \lambda_Z^0 = 0$, SM $WW\gamma$ couplings). For simplicity, only one anomalous coupling at a time is allowed to differ from its SM value. The figure shows that at the Tevatron center-of-mass energy, NLO QCD corrections do not have a large influence on the sensitivity of the $p_T(e)$ distribution to anomalous couplings. The $O(\alpha_s)$ corrections at Tevatron energies are approximately 30–40% for the SM as well as for the anomalous coupling cases. Because of the larger coupling of the Z boson to quarks and W bosons [see Eq. (1)], anomalous WWZ couplings yield larger differences from the SM than nonstandard $WW\gamma$ couplings of the same type and strength. Whereas terms proportional to λ_V and $\Delta\kappa_V$ in the helicity amplitudes grow like $\hat{s}/M_W^2$, terms associated with Δg_1^Z only increase with $\sqrt{\hat{s}}/M_W$ [1]. As a result, the sensitivity of W^+W^- production to nonstandard values of g_1^Z is considerably smaller than it is for $\Delta\kappa_V$ and λ_V.

For $\Delta\kappa_V^0$ (Δg_1^{Z0}), positive anomalous couplings lead to $\sim 40\%$ ($\sim 20\%$) smaller deviations from the SM prediction in the $p_T(e)$ distribution than negative nonstandard couplings of equal magnitude, whereas the sign makes little difference for λ_V^0. This statement also applies to other distributions. This effect can be easily understood from the high energy behavior of the W^+W^- production amplitudes, $\mathcal{M}(\lambda_{W^+}, \lambda_{W^-})$, where $\lambda_{W^\pm}$ denotes the helicity of the $W^\pm$ boson [1]. Any dependence of the differential cross section on the sign of one of the anomalous coupling parameters originates from interference effects between the SM and the anomalous terms in the helicity amplitudes. In the SM, only $\mathcal{M}(\pm, \mp)$ and $\mathcal{M}(0, 0)$ remain finite for $\hat{s} \to \infty$. Contributions to the helicity amplitudes proportional to λ_V mostly influence the $(\pm, \pm)$ amplitudes. The SM $\mathcal{M}(\pm, \pm)$ amplitudes vanish like $1/\hat{s}$, and the nonstandard terms dominate except for the threshold region, $\sqrt{\hat{s}} \approx 2M_W$. For nonstandard values of λ_V, the cross section therefore depends only very little on the sign of the anomalous coupling. Terms proportional to $\Delta\kappa_V$ also increase like $\hat{s}/M_W^2$ with energy, but mostly contribute to the $(0,0)$ amplitude, which remains
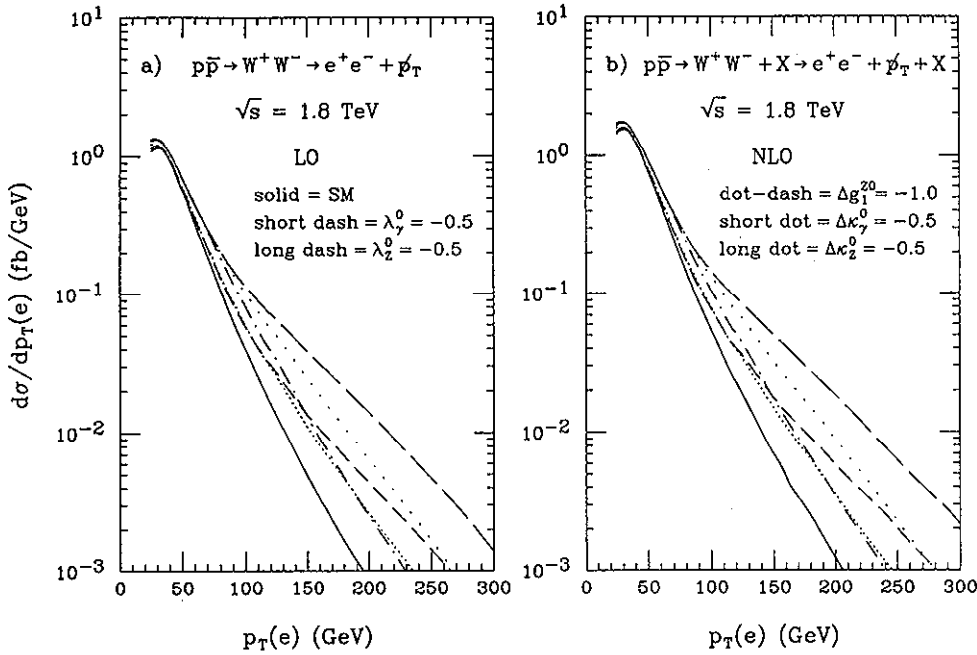
FIG. 2. The inclusive differential cross section for the electron transverse momentum in the reaction $p\bar{p} \to W^+W^- +X \to e^+e^-\not{p}_T + X$ at $\sqrt{s} = 1.8$ TeV; (a) in the Born approximation and (b) including NLO QCD corrections. The curves are for the SM (solid lines), $\lambda_\gamma^0 = -0.5$ (short dashed lines), $\Delta\kappa_\gamma^0 = -0.5$ (short dotted lines), $\lambda_Z^0 = -0.5$ (long dashed lines), $\Delta\kappa_Z^0 = -0.5$ (long dotted lines), and $\Delta g_1^{Z0} = -1.0$ (dot-dashed lines). The cuts imposed are summarized in Sec. III B.

finite in the SM in the high energy limit. Interference effects between the SM and the anomalous contributions to the (0,0) amplitude, thus are nonnegligible, resulting in a significant dependence of the differential cross section on the sign of $\Delta\kappa_V$. Finally, terms proportional to Δg_1^Z are proportional to $\sqrt{\hat{s}}/M_W$ and mostly influence the amplitudes with one longitudinal and one transverse W boson. In the SM, these terms vanish like $1/\sqrt{\hat{s}}$. The dependence on the sign of Δg_1^Z is, therefore, less pronounced than for $\Delta\kappa_V$.

The $p_T(e)$ distribution at the LHC is shown in Fig. 3. At leading-order, the sensitivity of the electron transverse momentum distribution to anomalous WWV couplings is

significantly more pronounced than at the Tevatron. Because of the form factor parameters assumed, the result for $\Delta g_1^{Z0} = -1$ approaches the SM result at large values of $p_T(e)$. As mentioned before, we have used $n = 2$ and a form factor scale of $\Lambda_{FF} = 1$ TeV in all our numerical simulations [see Eq. (8)]. For a larger scale Λ_{FF}, the deviations from the SM result become more pronounced at high energies. In contrast to the situation encountered at the Tevatron, the shape of the SM $p_T(e)$ spectrum at the LHC is considerably affected by NLO QCD corrections. At $p_T(e) = 600$ GeV, the QCD corrections increase the SM cross section by about a factor 4, whereas the enhancement is only a factor 1.5 at $p_T(e) = 100$ GeV. In
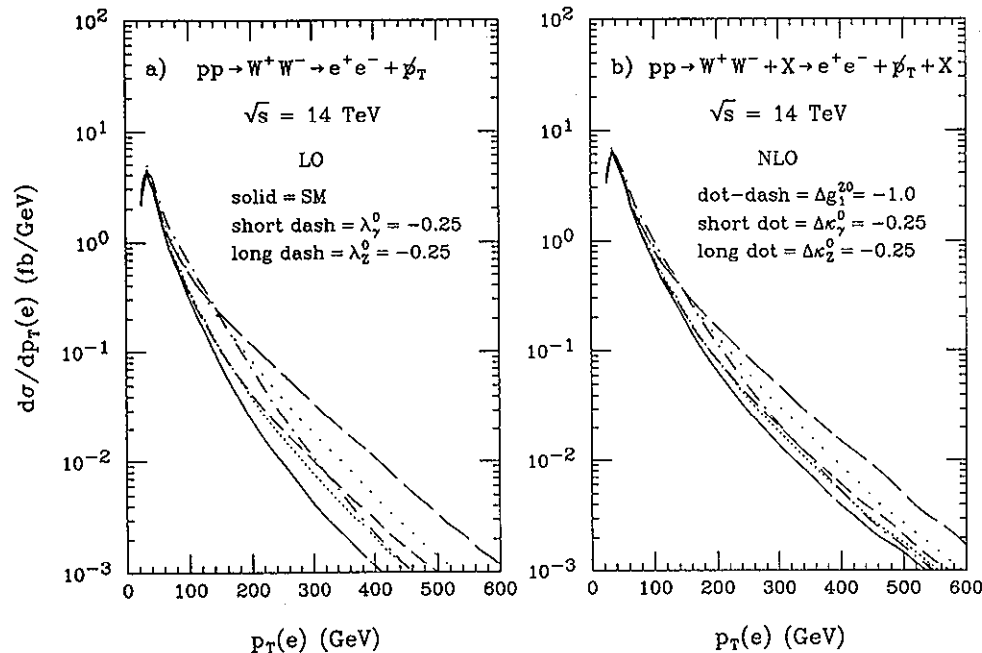

FIG. 3. The inclusive differential cross section for the electron transverse momentum in the reaction $pp \to W^+W^- + X \to e^+e^-\not{p}_T +X$ at $\sqrt{s} = 14$ TeV; (a) in the Born approximation and (b) including NLO QCD corrections. The curves are for the SM (solid lines), $\lambda_\gamma^0 = -0.25$ (short dashed lines), $\Delta\kappa_\gamma^0 = -0.25$ (short dotted lines), $\lambda_Z^0 = -0.25$ (long dashed lines), $\Delta\kappa_Z^0 = -0.25$ (long dotted lines), and $\Delta g_1^{Z0} = -1.0$ (dot-dashed lines). The cuts imposed are summarized in Sec. III B.

the presence of anomalous couplings, the higher order QCD corrections are much smaller than in the SM. In regions where the anomalous terms dominate, the $O(\alpha_s)$ corrections are typically between 30% and 40%. At next-to-leading-order, the sensitivity of the electron transverse momentum spectrum to anomalous couplings thus is considerably reduced at the LHC.

The large QCD corrections at high values of $p_T(e)$ are caused by a collinear enhancement factor, $\log^2[p_T(W)/M_W]$, in the $qg \to W^+W^-q$ partonic cross section for W transverse momenta much larger than M_W, $p_T(W) \gg M_W$, and the large qg luminosity at LHC energies [12]. It arises from the kinematical region where one of the W bosons is produced at large p_T and recoils against the quark, which radiates a soft W boson which is almost collinear to the quark, and thus is similar in nature to the enhancement of QCD corrections observed at large photon and Z boson transverse momenta in $W\gamma$ and WZ production [57–59]. Since the Feynman diagrams contributing in the collinear approximation do not involve the WWV vertices, the logarithmic enhancement factor only affects the SM matrix elements.

Although nonstandard WWV couplings lead to a large enhancement in the differential cross section of the lepton transverse momentum in $W^+W^- \to \ell_1^+\ell_2^- \not{p}_T$ production, the sensitivity is, because of the phase space effect of the W decays, significantly reduced compared to that of the photon (Z) transverse momentum distribution in $W\gamma$ (WZ) production [58,59]. As an alternative to the averaged charged lepton p_T distribution, the differential cross sections of the maximum and minimum lepton transverse momenta can be studied. The distribution of the maximum lepton p_T exhibits a sensitivity to nonstandard WWV couplings similar to that encountered in the average lepton p_T distribution. The minimum lepton transverse momentum distribution, on the other hand, is very insensitive to anomalous couplings. In contrast to the charged lepton p_T distribution, the shape of the invariant mass spectrum of the e^+e^- pair remains essentially unaffected by QCD corrections. However, the $M(e^+e^-)$ distribution is found to be considerably less sensitive to anomalous WWV couplings than the transverse momentum spectrum of the charged leptons. The cluster transverse mass distribution exhibits a sensitivity to nonstandard WWV couplings which is quite similar to that found in the $p_T(e)$ distribution.

In Figs. 4 and 5 we show the differential cross section for the transverse momentum of the charged lepton pair, which we denote by $p_T(e^+e^-)$ $[p_T(e^+e^-) \equiv \mathbf{p}_T(e^+) + \mathbf{p}_T(e^-)]$. The leading-order $p_T(e^+e^-)$ spectrum is seen to be considerably more sensitive to nonstandard WWV couplings than the $p_T(e)$ distribution. QCD corrections strongly affect the shape of the $p_T(e^+e^-)$ distribution, and reduce the sensitivity to anomalous couplings. At the LHC this effect is very dramatic (see Fig. 5); the NLO lepton pair p_T spectrum is seen to be considerably less sensitive to nonstandard WWV couplings than the NLO $p_T(e)$ distribution [see Fig. 3(b)].

The effect of the QCD corrections is shown in more detail in Fig. 6, where we display the ratio of the NLO and LO differential cross sections for the transverse momentum of the charged leptons and the pair. Both at Tevatron and LHC energies, the $O(\alpha_s)$ corrections are approximately 20–30% at small $p_T(e^+e^-)$ values. The NLO to LO differential cross section ratio begins to rise rapidly for $p_T(e^+e^-) > 70$ GeV, and for $p_T(e^+e^-) = 200$ GeV (600 GeV) the QCD corrections increase the cross section by a factor ~ 6 (~ 100) at the Tevatron (LHC). The shape change in the $p_T(e^+e^-)$ distribution thus is much more pronounced than that observed in the charged lep-
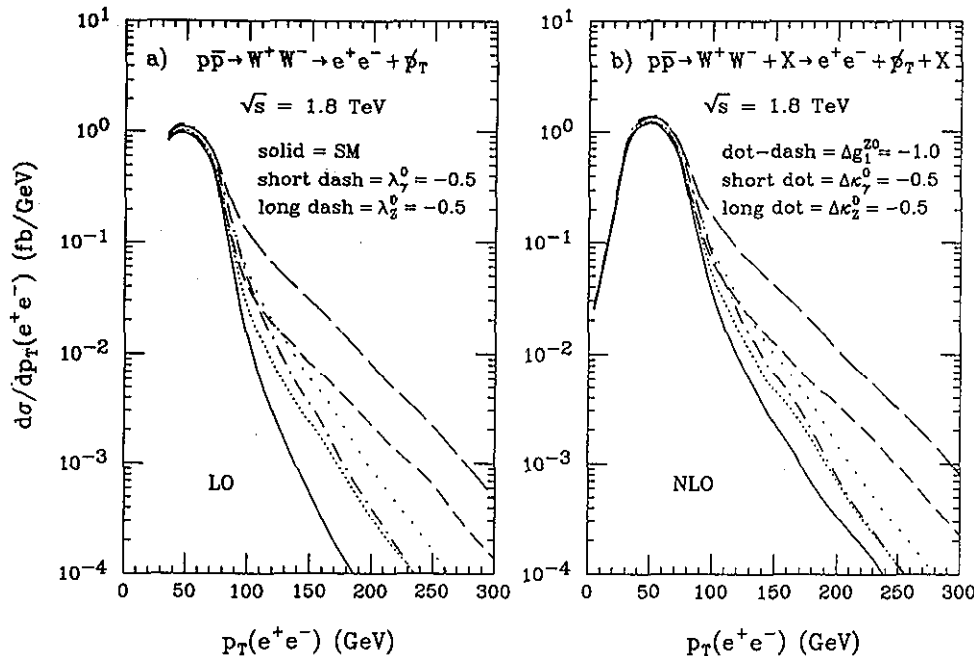

FIG. 4. The inclusive differential cross section for the transverse momentum of the charged lepton pair in the reaction $p\bar{p} \to W^+W^- + X \to e^+e^-\not{p}_T + X$ at $\sqrt{s} = 1.8$ TeV; (a) in the Born approximation and (b) including NLO QCD corrections. The curves are for the SM (solid lines), $\lambda_\gamma^0 = -0.5$ (short dashed lines), $\Delta\kappa_\gamma^0 = -0.5$ (short dotted lines), $\lambda_Z^0 = -0.5$ (long dashed lines), $\Delta\kappa_Z^0 = -0.5$ (long dotted lines), and $\Delta g_1^{Z0} = -1.0$ (dot-dashed lines). The cuts imposed are summarized in Sec. III B.
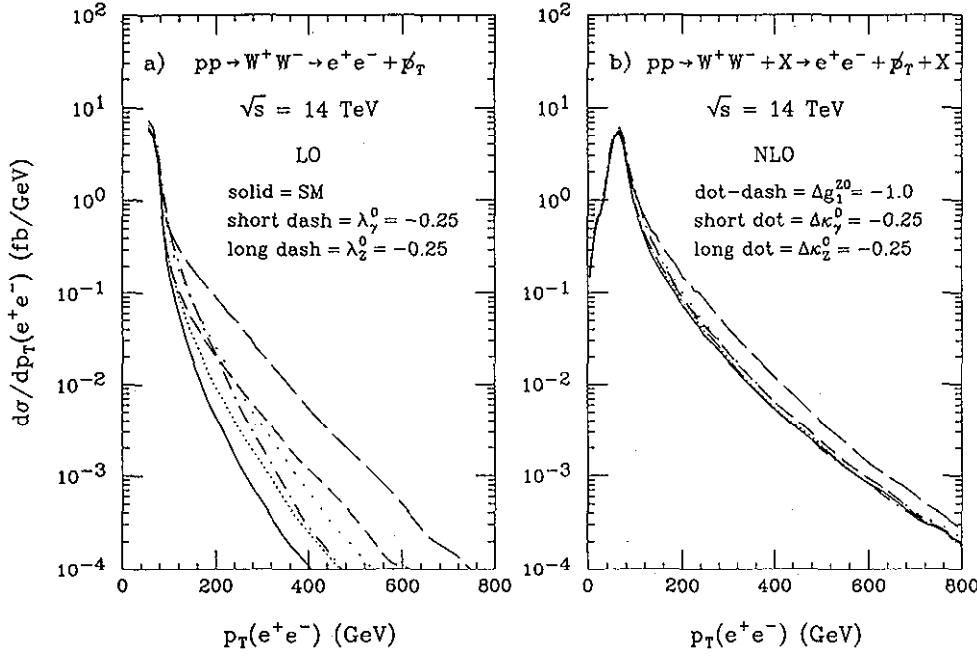
FIG. 5. The inclusive differential cross section for the transverse momentum of the charged lepton pair in the reaction $pp \to W^+W^- + X \to e^+e^-\not{p}_T + X$ at $\sqrt{s} = 14$ TeV; (a) in the Born approximation and (b) including NLO QCD corrections. The curves are for the SM (solid lines), $\lambda_\gamma^0 = -0.25$ (short dashed lines), $\Delta\kappa_\gamma^0 = -0.25$ (short dotted lines), $\lambda_Z^0 = -0.25$ (long dashed lines), $\Delta\kappa_Z^0 = -0.25$ (long dotted lines), and $\Delta g_1^{Z0} = -1.0$ (dot-dashed lines). The cuts imposed are summarized in Sec. III B.

ton transverse momentum distribution.

In the SM, the dominant $W^\pm$ helicity at high energies in $\bar{u}u \to W^+W^-$ ($\bar{d}d \to W^+W^-$) is $\lambda_{W^\pm} = \mp 1$ ($\lambda_{W^\pm} = \pm 1$) [1,5,17] because of a t-channel pole factor which peaks at small scattering angles with an enhancement factor which is proportional to $\hat{s}$. Because of the $V - A$ nature of the $We\nu$ coupling, the angular distribution of the lepton in the rest frame of the parent W is proportional to $(1 + Q_W\lambda_W\cos\theta)^2$, where Q_W is the W charge and θ is the angle with respect to the flight direction of the W in the parton center-of-mass frame. As a result, the charged leptons tend to be emitted either

both into ($\bar{d}d$ annihilation), or both against the flight direction of their parent W boson ($\bar{u}u$ annihilation), i.e., they reflect the kinematical properties of the W bosons. At leading-order, the W^+ and the W^- in W pair production are back to back in the transverse plane, and the transverse momenta of the two leptons tend to cancel at high energies. Above the W threshold, the SM $p_T(e^+e^-)$ distribution thus drops much more rapidly than the p_T distribution of the charged leptons.

Anomalous WWV couplings tend to destroy the correlation of the charged lepton momenta. Nonstandard values of $\Delta\kappa_V$ mostly contribute to the amplitude where
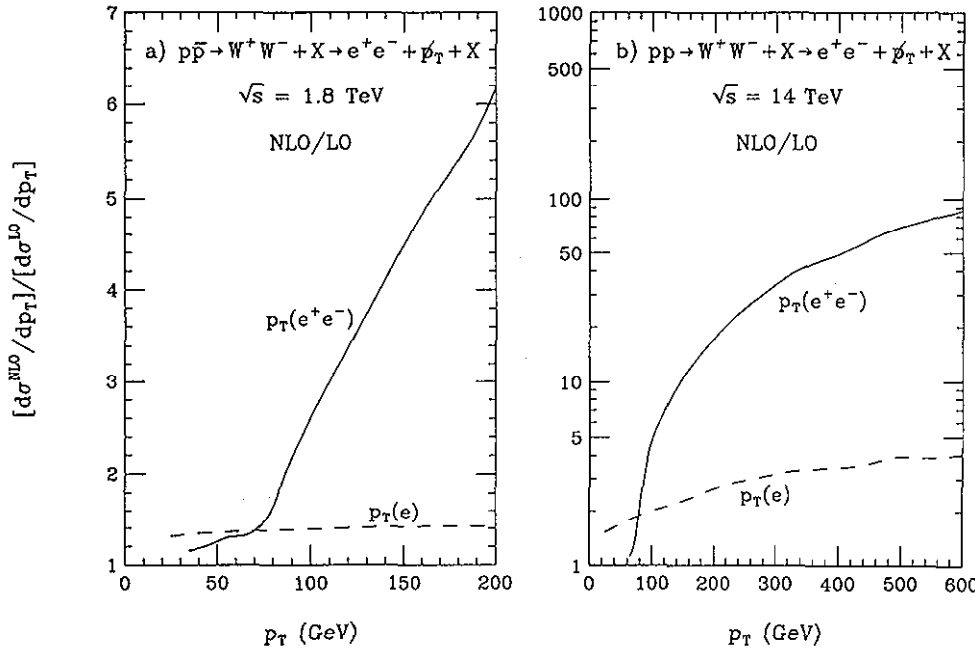

FIG. 6. Ratio of the NLO and LO differential cross sections of the transverse momenta of the charged leptons (dashed lines) and the lepton pair (solid lines) in the SM as a function of p_T for (a) $p\bar{p} \to W^+W^- + X \to e^+e^-\not{p}_T + X$ at $\sqrt{s} = 1.8$ TeV; and (b) $pp \to W^+W^- + X \to e^+e^-\not{p}_T + X$ at $\sqrt{s} = 14$ TeV. The cuts imposed are summarized in Sec. III B.

both W's are longitudinal. Terms in the helicity amplitudes proportional to Δg_1^Z predominantly affect the $(0,\pm)$ and $(\pm,0)$ amplitudes, and nonzero values of λ_V mostly contribute to $(\pm,\pm)$ states, with equal numbers of W's of positive and negative helicity [1]. The angular distribution of the W decay lepton for a longitudinal W boson is proportional to $\sin^2\theta$, whereas equal numbers of W's with $\lambda_W = +1$ and $\lambda_W = -1$ produce a $(1 + \cos^2\theta)$ spectrum. As a result, the cancellation of the transverse momenta of the leptons is less perfect in the presence of anomalous couplings. This reinforces the growth of the nonstandard contributions to the helicity amplitudes with energy, thus producing a very pronounced sensitivity of the LO $p_T(e^+e^-)$ distribution to anomalous WWV couplings.

The delicate balance of the lepton transverse momenta, however, is also spoiled by the real emission processes ($q\bar{q} \to W^+W^-g$ etc.) which contribute to the $O(\alpha_s)$ QCD corrections. At large transverse momenta, QCD corrections therefore affect the $p_T(e^+e^-)$ distribution much more than the $p_T(e)$ spectrum; see Fig. 6.

At lowest order, the p_T vector of the charged lepton pair, is balanced by the missing transverse momentum $\not{p}_T$, vector which results from the two neutrinos which are not observed in the detector. The angular distribution of the neutrinos in the rest frame of the parent W can be obtained from that of the charged leptons by replacing the angle θ by $\pi + \theta$. As a result, the neutrino transverse momentum vectors are also strongly correlated. The $\not{p}_T$ differential cross section is therefore expected to exhibit a sensitivity to anomalous WWV couplings and $O(\alpha_s)$ QCD corrections similar to that of the $p_T(e^+e^-)$ distribution. At high values of $\not{p}_T$, the missing transverse momentum spectrum is found to be very similar to the $p_T(e^+e^-)$ distribution, with a similar sensitivity to anomalous WWV couplings and to $O(\alpha_s)$ QCD corrections. At small values, the LO $p_T(e^+e^-)$ and $\not{p}_T$

distributions differ because of the smearing imposed on the charged lepton momenta. Experimentally, the missing transverse momentum distribution is more difficult to measure than the $p_T(e^+e^-)$ differential cross section because of cracks and other detector imperfections which give rise to "fake" $\not{p}_T$, or worsen the resolution of the missing p_T distribution.

From the picture outlined above, one expects that at next-to-leading order, W^+W^- events with a large missing transverse momentum or a high p_T charged lepton pair, will most of the time contain a high transverse momentum jet. This fact is illustrated in Fig. 7 which shows the decomposition of the inclusive SM NLO $p_T(e^+e^-)$ differential cross section into NLO 0 jet and LO 1 jet exclusive cross sections at the Tevatron and LHC. For comparison, the $p_T(e^+e^-)$ distribution obtained in the Born approximation is also shown in the figure. Here, a jet is defined as a quark or gluon with

$$p_T(j) > 20 \text{ GeV} \quad \text{and} \quad |\eta(j)| < 2.5 \quad (12)$$

at the Tevatron, and

$$p_T(j) > 50 \text{ GeV} \quad \text{and} \quad |\eta(j)| < 3 \quad (13)$$

at the LHC. The sum of the NLO 0 jet and the LO 1 jet exclusive cross section is equal to the inclusive NLO cross section. The results for the NLO exclusive $W^+W^- + 0$ jet and the LO exclusive $W^+W^- + 1$ jet differential cross sections depend explicitly on the jet definition. Only the inclusive NLO distributions are independent of the jet definition.

Present LHC studies [54,55,60] and projections to Tevatron energies suggest that jets fulfilling the criteria of Eqs. (12) and (13) can be identified without problems at the TeV* [14] and LHC [15] design luminosities of 10^{33} cm^{-2} s^{-1} and 10^{34} cm^{-2} s^{-1}, respectively. For luminosities significantly below the design luminosity, it
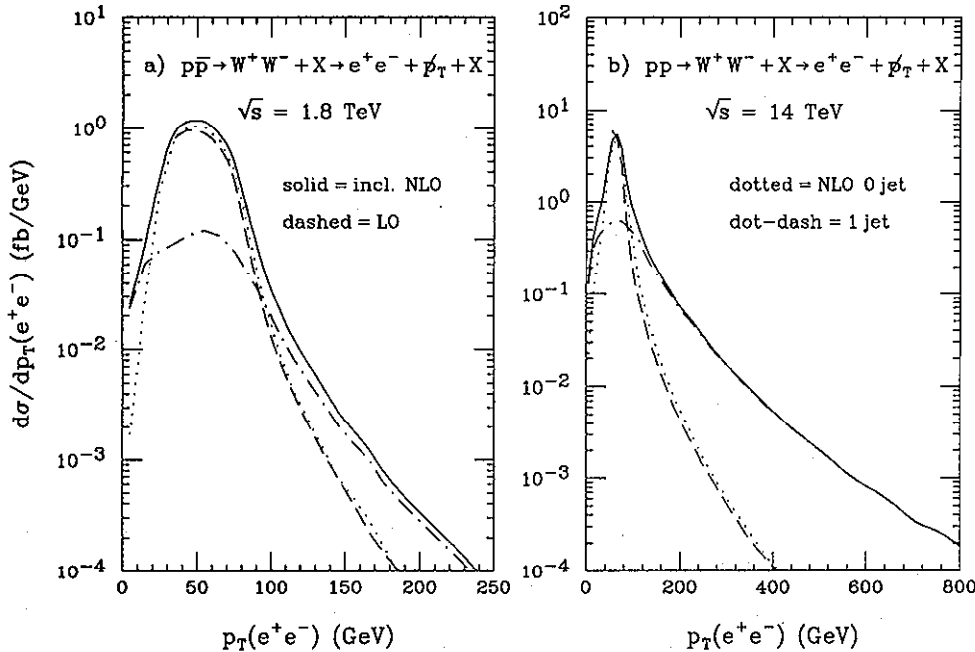

FIG. 7. The $p_T(e^+e^-)$ differential cross sections for (a) $p\bar{p} \to W^+W^- + X \to e^+e^-\not{p}_T + X$ at $\sqrt{s} = 1.8$ TeV; and (b) $pp \to W^+W^- + X \to e^+e^-\not{p}_T + X$ at $\sqrt{s} = 14$ TeV. The inclusive NLO differential cross section (solid line) is decomposed into the $O(\alpha_s)$ 0 jet (dotted line) and LO 1 jet (dot-dashed line) exclusive differential cross sections. For comparison, the Born cross section (dashed line) is also shown. The cuts imposed are summarized in Sec. III B. For the jet definitions, we have used Eqs. (12) and (13).

may well be possible to lower the jet-defining p_T threshold to 10 GeV at the Tevatron and 30 GeV at the LHC. It should be noted, however, that for theoretical reasons, the jet transverse momentum threshold cannot be made arbitrarily small in our calculation. For transverse momenta below 5 GeV (20 GeV) at the Tevatron (LHC), soft gluon resummation effects are expected to significantly change the shape of the jet p_T distribution [61]. For the jet definitions discussed above, these effects are expected to be unimportant and therefore are ignored in our calculation.

Figure 7 shows that at the Tevatron, the 1 jet cross section is larger than the 0 jet rate for $p_T(e^+e^-) > 100$ GeV, and dominates completely at large $p_T(e^+e^-)$. The NLO 0 jet and Born differential cross sections deviate by at most 30% for lepton pair transverse momenta above 30 GeV (60 GeV) at the Tevatron (LHC). For $p_T(e^+e^-) < 25$ GeV (40 GeV) at the Tevatron (LHC), the 1 jet cross section again dominates. In this region the 0 jet cross section is strongly suppressed because of the cut imposed on the missing transverse momentum. Figure 7 suggests that the size of the QCD corrections in the $p_T(e^+e^-)$ distribution can be dramatically reduced by vetoing hard jets in the central rapidity region, i.e., by imposing a "zero jet" requirement and considering the $W^+W^- + 0$ jet channel only.

As mentioned in Sec. III A, all our results are obtained for $Q^2 = M_{WW}^2$. The Born cross section for W pair production depends significantly on the choice of Q, which enters through the scale dependence of the parton distribution functions. At the NLO level, the Q dependence enters not only via the parton distribution functions, but also through the running coupling $\alpha_s(Q^2)$ and the explicit factorization scale dependence in the order $\alpha_s(Q^2)$ correction terms. Similar to the situation encountered in $W\gamma$ and WZ production in hadronic collisions [58,59], we find that the NLO $W^+W^- + 0$ jet exclusive cross section is almost independent of the scale Q. Here, the scale dependence of the parton distribution functions is compensated by that of $\alpha_s(Q^2)$ and the explicit factorization scale dependence in the correction terms. The Q dependence of the inclusive NLO cross section is significantly larger than that of the NLO 0 jet cross section; it is dominated by the 1 jet exclusive component which is calculated only to lowest order and thus exhibits a considerable scale dependence.

E. Background processes

So far, we have only considered the $W^+W^- \to e^+e^- p\!\!\!/_T + X$ signal cross section. However, a number of processes lead to the same final states. These processes contribute to the background and, in addition to the NLO QCD corrections, reduce the sensitivity to anomalous WWV couplings. The situation is summarized in Fig. 8, where we show, at leading-order, the transverse momentum distribution of the charged lepton pair for the W^+W^- signal (solid lines), and the most important
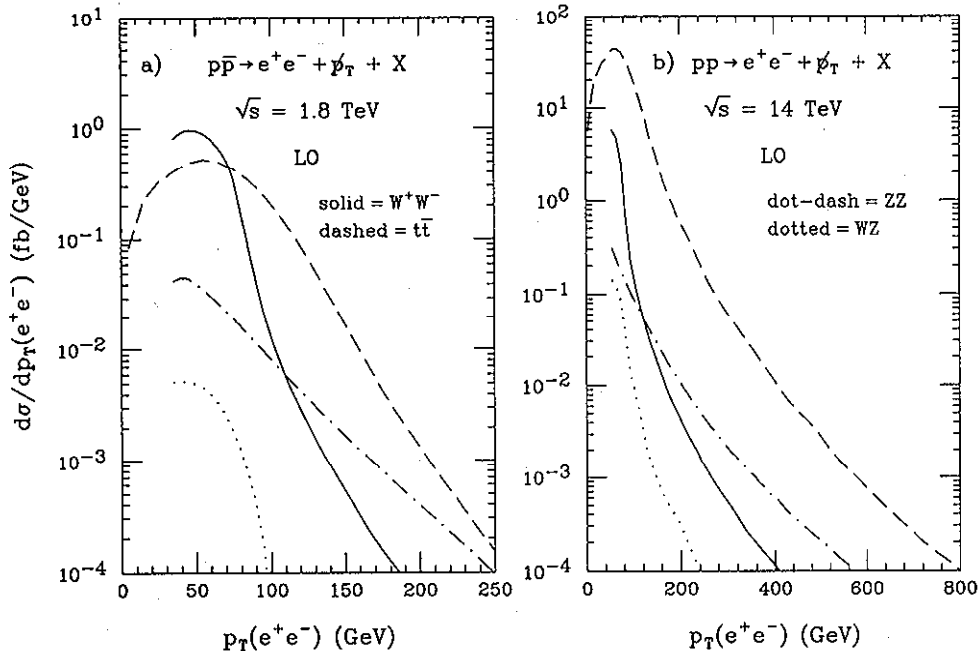

FIG. 8. The LO differential cross sections for the e^+e^- transverse momenta for (a) $p\bar{p} \to e^+e^- p\!\!\!/_T + X$ at $\sqrt{s} = 1.8$ TeV; and (b) $pp \to e^+e^- p\!\!\!/_T + X$ at $\sqrt{s} = 14$ TeV. The SM W^+W^- cross section (solid line) is shown, together with the $t\bar{t} \to W^+W^- b\bar{b} \to e^+e^- p\!\!\!/_T + X$ rate for $m_t = 176$ GeV (dashed line), the $ZZ \to e^+e^- p\!\!\!/_T + X$ cross section (dot-dashed line), and the $W^\pm Z \to e^+e^- p\!\!\!/_T + X$ cross section where one of the two like sign charged leptons is produced with a rapidity outside the range covered by the detector (dotted line). The cuts imposed are summarized in Secs. III B and III D.

background processes.

The potentially most dangerous background originates from top quark pair production, $p\overset{(-)}{p} \to t\bar{t} \to W^+W^-b\bar{b} \to e^+e^-\not{p}_T + X$. To compute the top quark production rate, we use the matrix elements of the full processes $q\bar{q}$, $gg \to t\bar{t} \to W^+W^-b\bar{b} \to f_1\bar{f}_2f_3\bar{f}_4b\bar{b}$ [62]. We assume that the SM correctly describes the production and decay of top quarks. The current top quark masses obtained by CDF and D0 are $m_t = 176 \pm 8 \pm 10$ GeV [46] and $m_t = 199^{+19}_{-21} \pm 22$ GeV [47], respectively. In the following, for definiteness, we take $m_t = 176$ GeV. For larger values of m_t, the top quark background is reduced; the $t\bar{t}$ cross section drops by about a factor of 2 (1.7) at the Tevatron (LHC) if the top quark mass is increased to 200 GeV.

For the cuts we impose (see Sec. III A), the W^+W^- and $t\bar{t}$ total cross sections are approximately equal at the Tevatron. However, because of the b quarks produced in the decay of the t and $\bar{t}$, the $p_T(e^+e^-)$ distribution from $t\bar{t}$ production is considerably broader and harder than that of the charged lepton pair in W^+W^- production. At large values of $p_T(e^+e^-)$, the top quark background (dashed line), therefore, completely dominates over the W pair signal at the Tevatron. At the LHC, the $t\bar{t}$ cross section is approximately a factor 25 larger than the W^+W^- rate, and the top quark background is at least a factor 10 bigger than the signal over the entire range of lepton pair transverse momenta [see Fig. 8(b)]. For $m_t = 200$ GeV, the $p_T(e^+e^-)$ differential cross section almost coincides with that obtained for $m_t = 176$ GeV for $p_T(e^+e^-) > 150$ GeV; only for smaller values of the lepton pair transverse momentum does the larger mass reduce the rate.

$W^{\pm}Z$ production where both the W and the Z boson decay leptonically may also contribute to the background if one of the two like sign charged leptons is produced with a rapidity outside the range covered by the detector. To estimate the $W^{\pm}Z$ background, we have assumed that, at the Tevatron (LHC), charged leptons with $p_T(\ell) < 10$ GeV (15 GeV) or $|\eta(\ell)| > 2.5$ (3.0) are not detected, and thus contribute to the missing transverse momentum vector. Our results, represented by the dotted lines in Fig. 8, show that the $W^{\pm}Z$ background is unlikely to be a problem in W^+W^- production. For the cuts chosen, it is at least one order of magnitude smaller than the W^+W^- signal.

The top quark and $W^{\pm}Z$ backgrounds contribute to $\ell_1^+\ell_2^-\not{p}_T + X$ production for all lepton flavor combinations, $\ell_{1,2} = e, \mu$. Other background processes such as ZZ production where one of the Z bosons decays into charged leptons, $Z \to \ell^+\ell^-$, and the other into neutrinos, $Z \to \bar{\nu}\nu$, contribute only for $\ell_1 = \ell_2$. The transverse momentum distribution of the charged lepton pair in $ZZ \to e^+e^-\not{p}_T + X$ is given by the dot-dashed lines in Fig. 8. The $p_T(e^+e^-)$ distribution from ZZ production is seen to be significantly harder than that from $p\overset{(-)}{p} \to W^+W^-$. For $p_T(e^+e^-)$ values larger than about 120 GeV, the ZZ background is larger than the W^+W^- signal, thus reducing the sensitivity to anomalous WWV couplings.

Backgrounds where the $\ell^+\ell^-$ pair originates from a Z boson can be easily suppressed by requiring that

$$|m(\ell^+\ell^-) - M_Z| > 10 \text{ GeV}. \tag{14}$$

While this cut almost completely eliminates those background processes, it hardly affects the W^+W^- signal. The effect of the $m(e^+e^-)$ cut is particularly small at high $p_T(e^+e^-)$ values, and therefore does not noticeably influence the sensitivity to anomalous WWV couplings.

Numerous other processes contribute to the background in the $\ell_1^+\ell_2^-\not{p}_T + X$ channels. In order not to overburden the figure, the $p_T(e^+e^-)$ differential cross sections from these processes are not included in Fig. 8. The rate for associated production of W bosons and top quarks, $p\overset{(-)}{p} \to W^-t + X$, $W^+\bar{t} + X \to \ell_1^+\ell_2^-\not{p}_T + X$, is about a factor 50 (100) smaller than the $t\bar{t}$ cross section at the Tevatron (LHC) [63,64] and therefore does not represent a problem. Because of the relatively high lepton and missing transverse momentum cuts we impose (see Sec. III A), the $Z + X \to \tau^+\tau^- + X \to e^+e^-\not{p}_T + X$ background is substantially suppressed. Furthermore, the $p_T(e^+e^-)$ distribution from $Z \to \tau^+\tau^-$ decays falls very steeply; for $p_T(e^+e^-) > 50$ GeV the Z boson must either be far off shell, or be accompanied by a high p_T jet. Using the "poor man's shower" approach [65] to simulate the transverse motion of the Z boson, we find that the $Z + X \to \tau^+\tau^- + X \to e^+e^-\not{p}_T + X$ background to be at least a factor 5 (10) smaller than the W^+W^- signal at the Tevatron (LHC) over the entire $p_T(e^+e^-)$ range. The background from $b\bar{b}$, $c\bar{c}$, $Wg \to t\bar{b}$ [66,67], $q\bar{q}' \to t\bar{b}$ [67,68], Wc [69], or $Wb\bar{b}$, $Wc\bar{c}$ production is negligible (small) at the Tevatron [46,47,70] (LHC [54,63]) after lepton isolation cuts are imposed.

In contrast to the charm and bottom background, the top quark background is only insignificantly reduced by lepton isolation cuts. However, the b quarks produced in top quark decays frequently lead to one or two hadronic jets [71], and a 0 jet requirement can be used to suppress the $t\bar{t}$, as well as the $Wt + X$, rate. The decomposition of the $p_T(e^+e^-)$ differential cross section in $t\bar{t}$ production at lowest order into 0 jet, 1 jet, and 2 jet exclusive cross sections at the Tevatron and LHC for $m_t = 176$ GeV is shown in Fig. 9, using the jet definitions of Eqs. (12) and (13) together with a jet clustering algorithm. The clustering algorithm merges the b and $\bar{b}$ quark into one jet if their separation is $\Delta R(b,\bar{b}) < 0.4$ and their combined transverse momentum is larger than the jet-defining p_T threshold. At Tevatron energies, $t\bar{t}$ production predominantly leads to $W^+W^- + 2$ jet events. Less than 1% of the events have no jet with $p_T(j) > 20$ GeV. At the LHC, approximately 10% of all events have no jet with a transverse momentum in excess of 50 GeV.

As an alternative to a jet veto, a cut on the transverse momentum of the hadrons, $p_T(h)$, can be imposed in order to suppress the top quark background [10]. The transverse momentum vector of the hadrons is related to the other transverse momenta in an $e^+e^-\not{p}_T + X$ event through the equation
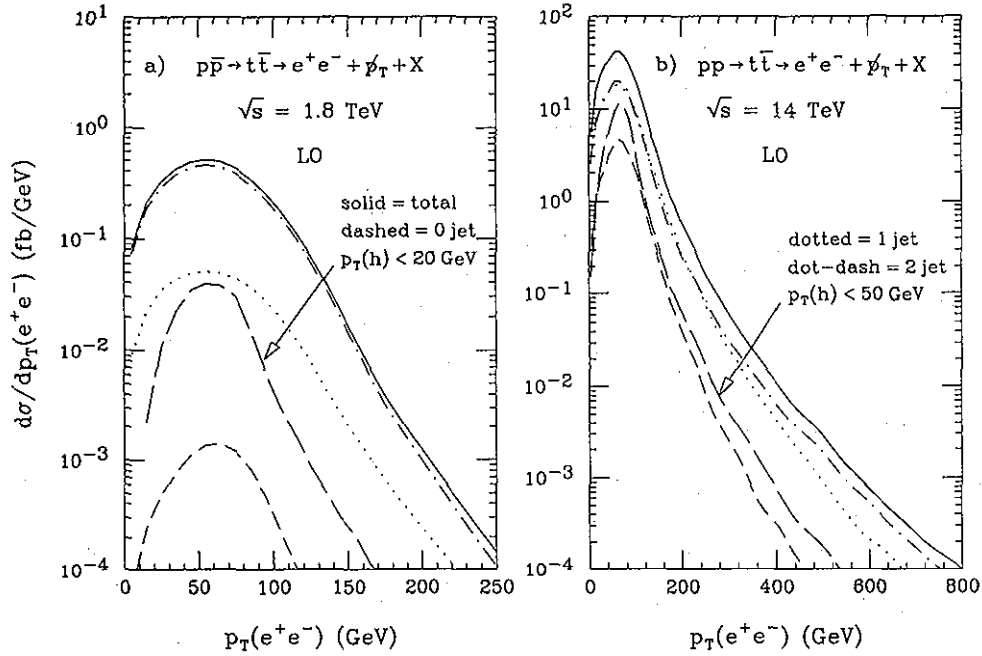
FIG. 9. The LO differential cross sections for the e^+e^- transverse momenta for (a) $p\bar{p} \to t\bar{t} \to e^+e^-\not{p}_T + X$ at $\sqrt{s} = 1.8$ TeV; and (b) $pp \to t\bar{t} \to e^+e^-\not{p}_T + X$ at $\sqrt{s} = 14$ TeV. The solid lines show the inclusive differential cross sections. The dashed, dotted, and dot-dashed lines give the 0 jet, 1 jet, and 2 jet exclusive cross sections, respectively. The long dashed curves show the $p_T(e^+e^-)$ distribution with a cut on the total transverse momentum of the hadrons in the event of $p_T(h) < 20$ GeV (50 GeV) at the Tevatron (LHC) [see Eq. (15)]. We assume a top quark mass of $m_t = 176$ GeV. The cuts imposed are summarized in Sec. III B. For the jet definitions, we have used Eqs. (12) and (13).

$$\mathbf{p}_T(h) = -\left[\mathbf{p}_T(e^+) + \mathbf{p}_T(e^-) + \not{\mathbf{p}}_T\right]. \qquad (15)$$

In contrast to a jet veto requirement, a cut on $p_T(h)$ is independent of the jet definition, in particular the jet cone size. It also significantly reduces the dependence on the jet-energy corrections. For $t\bar{t}$ production in the dilepton channel, at LO, $p_T(h) = p_T(\bar{b}b)$, the transverse momentum of the $\bar{b}b$ pair. For $W^+W^- + X \to \ell_1^+\ell_2^-\not{p}_T + X$, at NLO, $p_T(h)$ coincides with the jet transverse momentum. In this case, a jet veto and a cut on $p_T(h)$ are equivalent.

The effect of a $p_T(h) < 20$ GeV (50 GeV) cut at the Tevatron (LHC) is shown by the long dashed lines in Fig. 9. Clearly, at the Tevatron the $p_T(h)$ cut is considerably less efficient than a 0 jet requirement with a cut on the jet p_T equal to the cut imposed on $p_T(h)$. At the LHC, the jet veto is only slightly more efficient than a cut on the transverse momentum of the hadrons. Results which are qualitatively very similar to those shown in Fig. 9 are obtained for $m_t = 200$ GeV.

In Fig. 10, we compare the $p_T(e^+e^-)$ differential cross section of the W^+W^- signal with the residual $t\bar{t}$ background at Tevatron and LHC energies for the jet definition of Eq. (12). A jet veto is seen to reduce the $t\bar{t}$ background at the Tevatron to a few percent of the signal [see Fig. 10(a)]. On the other hand, if a $p_T(h) < 20$ GeV cut is imposed, the top quark background is still about half as large as the W^+W^- signal in the high $p_T(e^+e^-)$ tail. For $p_T(h) < 10$ GeV, the $t\bar{t}$ rate is approximately one order of magnitude below the W^+W^- signal cross section.

At the LHC [Fig. 10(b)], neither a cut on the transverse momentum of the hadrons of $p_T(h) < 50$ GeV nor a jet veto with the same 50 GeV p_T threshold are sufficient to reduce the $t\bar{t}$ rate to below the W pair signal. If the threshold of the $p_T(h)$ or jet veto cut can be lowered to 30 GeV, the top quark background can be reduced by an additional factor 2 to 5. Nevertheless, the residual $t\bar{t}$ rate is still somewhat larger than the W^+W^- cross section for large values of $p_T(e^+e^-)$.

It is difficult to further reduce the top quark background at the LHC. Once a jet veto is imposed, the characteristics of W^+W^- signal and $t\bar{t}$ background events are very similar. To suppress the $t\bar{t}$ cross section to below the W^+W^- rate, one would need to reduce the transverse momentum threshold in the jet veto or the $p_T(h)$ cut to a value considerably below 30 GeV. This is probably only feasible if the LHC is operated significantly below its design luminosity of $\mathcal{L} = 10^{34}$ cm^{-2} s^{-1}.

In our estimate of the top quark background, we have calculated the $t\bar{t}$ cross section to lowest order in α_s. Higher order QCD corrections affect the $t\bar{t}$ differential cross sections only slightly [72] and therefore do not appreciably change the results shown in Figs. 8–10.

In Fig. 11, finally, we display the $p_T(e^+e^-)$ distribution for $p\overset{(-)}{p} \to e^+e^-\not{p}_T + 0$ jet where we have added the differential cross sections of the $W^+W^- + 0$ jet signal and the residual top quark background. Results are displayed for the SM and for anomalous WWV couplings in the HISZ scenario [27] (see Sec. II B). So far, in order to investigate
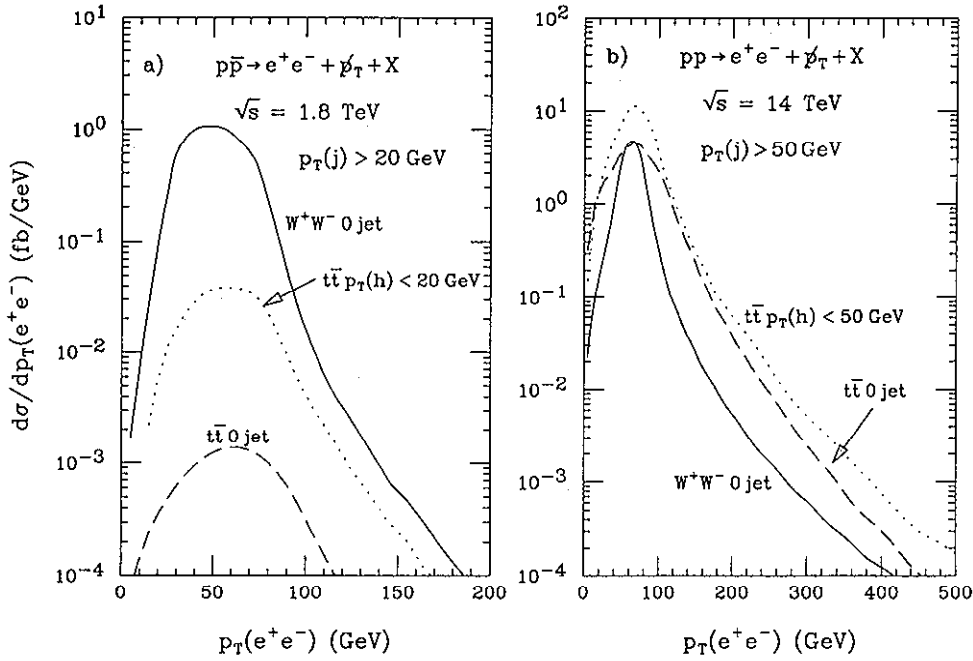
FIG. 10. The e^+e^- transverse momentum distribution for (a) $p\bar{p} \to e^+e^-\not{p}_T + X$ at $\sqrt{s} = 1.8$ TeV; and (b) $pp \to e^+e^-\not{p}_T + X$ at $\sqrt{s} = 14$ TeV. Shown are the differential cross sections for $W^+W^- + 0$ jet production at $O(\alpha_s)$ (solid line), $t\bar{t} \to e^+e^-\not{p}_T + 0$ jet (dashed line), and $t\bar{t} \to e^+e^-\not{p}_T + X$ with a $p_T(h)$ cut imposed (dotted line). At the Tevatron (LHC) a jet-defining p_T threshold of 20 GeV (50 GeV) is used. For W^+W^- production at $O(\alpha_s)$, a jet veto and a $p_T(h)$ cut are equivalent. The additional cuts imposed are summarized in Sec. III B.
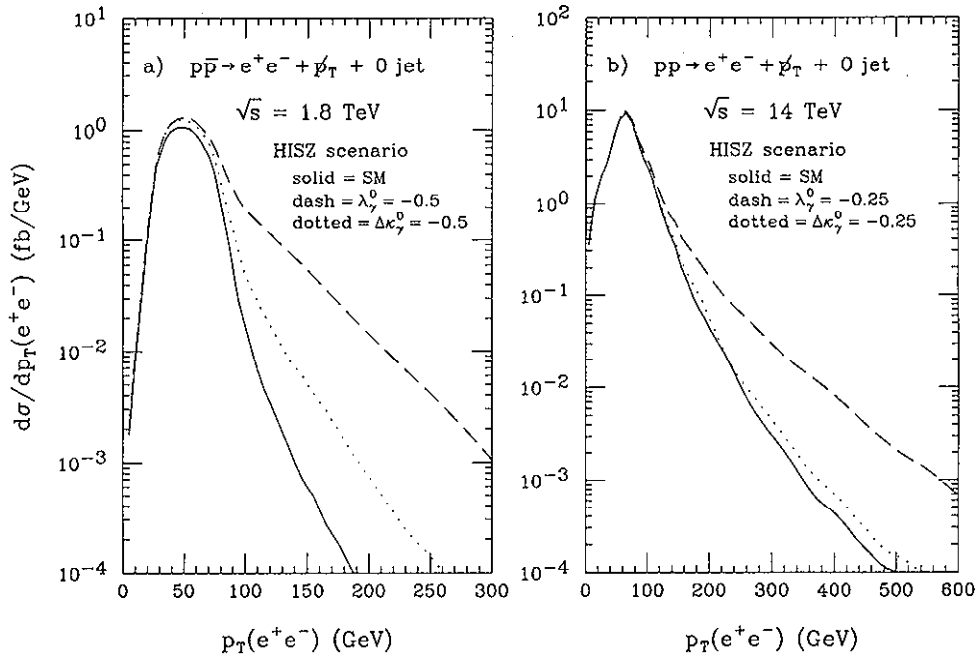

FIG. 11. The combined differential cross section for the e^+e^- transverse momenta from $W^+W^- \to e^+e^-\not{p}_T + 0$ jet and $t\bar{t} \to e^+e^-\not{p}_T + 0$ jet for (a) $p\bar{p}$ collisions at $\sqrt{s} = 1.8$ TeV, and (b) pp collisions at $\sqrt{s} = 14$ TeV. The curves are for the SM (solid line), and two sets of anomalous couplings in the HISZ scenario [Eqs. (9)–(11)]. The dashed line shows the result for $(\lambda_\gamma^0 = -0.5, \Delta\kappa_\gamma^0 = 0)$ [$(\lambda_\gamma^0 = -0.25, \Delta\kappa_\gamma^0 = 0)$] at the Tevatron [LHC]. The dotted line corresponds to $(\lambda_\gamma^0 = 0, \Delta\kappa_\gamma^0 = -0.5)$ [$(\lambda_\gamma^0 = 0, \Delta\kappa_\gamma^0 = -0.25)$]. The cuts imposed are summarized in Sec. III B. For the jet definitions, we have used Eqs. (12) and (13). A top quark mass of $m_t = 176$ GeV was used.

how the differential cross sections depend on the nonstandard WWV couplings, we have assumed that only one anomalous coupling at a time is nonvanishing. In a realistic model, there is no reason, however, to expect that this is the case. The scenario of Ref. [27] provides an example of a model in which both $WW\gamma$ and WWZ anomalous couplings are simultaneously nonzero, thus making it possible to study the interference effects between the different nonstandard couplings. Furthermore, the number of independent WWV couplings in this scenario can be reduced from five to two [see Eqs. (9)–(11)] by imposing one simple additional constraint. The dashed and dotted lines in Fig. 11 display the $p_T(e^+e^-)$ distribution of signal plus background for two sets of nonstandard couplings fulfilling Eqs. (9)–(11). For simplicity, only one of the two independent couplings is allowed to differ from its SM value at a time. The figure shows that at the Tevatron the sensitivity to anomalous WWV couplings remains virtually unaffected by the $t\bar{t} \rightarrow e^+e^-\not{p}_T + 0$ jet background, whereas it is significantly reduced at the LHC.

F. $W \rightarrow \tau\nu$ decay modes

So far we have completely ignored the contributions from decay modes where one or both charged leptons in the final state originate from $W \rightarrow \tau\nu_\tau \rightarrow e\nu_e\bar{\nu}_\tau\nu_\tau$. Experimentally, it is difficult to separate the $W \rightarrow \tau\nu$ and $W \rightarrow e\nu$ channels if the τ decays into leptons only. It is straightforward to implement τ decays into our calculation; one simply replaces the $W \rightarrow e\nu$ decay current, $J_\mu(k)$, with the $W \rightarrow \tau\nu_\tau \rightarrow e\nu_e\nu_\tau\nu_\tau$ decay current, $D_\mu^\tau(k)$.

In Fig. 12, we compare the LO $p_T(e^+e^-)$ spectrum of e^+e^- pairs where one (dashed lines) or both leptons (dotted lines) originate from τ decays with the distribution where both leptons originate from "prompt" $W \rightarrow e\nu$ decays. If both W's decay into τ leptons, the combined branching ratio of the subsequent τ decay, $[B(\tau \rightarrow e\nu_e\nu_\tau)]^2 \approx 0.032$, strongly suppresses the contribution of this channel. As a result, the $p_T(e^+e^-)$ differential cross section where both leptons originate from τ decays is approximately three orders of magnitude below that from prompt e^+e^- pairs. The slope of the $p_T(e^+e^-)$ distributions from $W^+W^- \rightarrow e^+\nu_e e^-\bar{\nu}_e$ and $W^+W^- \rightarrow \tau^+\nu_\tau\tau^-\bar{\nu}_\tau$ are similar.

However, this is not the case if only one of the two W bosons decays into $\tau\nu$. The charged lepton from the decaying τ lepton is typically much softer than that originating from $W \rightarrow e\nu$, thus spoiling the balance of the charged lepton transverse momenta. The resulting $p_T(e^+e^-)$ distribution is somewhat harder than that from $W^+W^- \rightarrow e^+\nu_e e^-\bar{\nu}_e$. While the rate of the τ decay mode is smaller by approximately one order of magnitude at low values of $p_T(e^+e^-)$, it is larger than the $W^+W^- \rightarrow e^+\nu_e e^-\bar{\nu}_e$ cross section for $p_T(e^+e^-) > 200$ GeV (250 GeV) at the Tevatron (LHC). Decay modes where one of the W bosons decays into $\tau\nu$ thus change the shape of the $p_T(e^+e^-)$ distribution, although considerably less than what the NLO QCD corrections do.

The NLO 0 jet e^+e^- transverse momentum distributions are very similar to the LO differential cross sections shown in Fig. 12. At the inclusive NLO level, or in the case of nonzero anomalous WWV couplings, the correlation of the charged lepton transverse momenta found in the SM LO $W^+W^- \rightarrow e^+\nu_e e^-\bar{\nu}_e$ case is not present and the $p_T(e^+e^-)$ differential cross section for $W^+W^- \rightarrow e^\pm\nu_e\tau^\mp\nu_\tau$ is about one order of magnitude below that from $W^+W^- \rightarrow e^+\nu_e e^-\bar{\nu}_e$ over the entire transverse momentum range considered. Contributions from channels where one W boson decays into a τ lepton
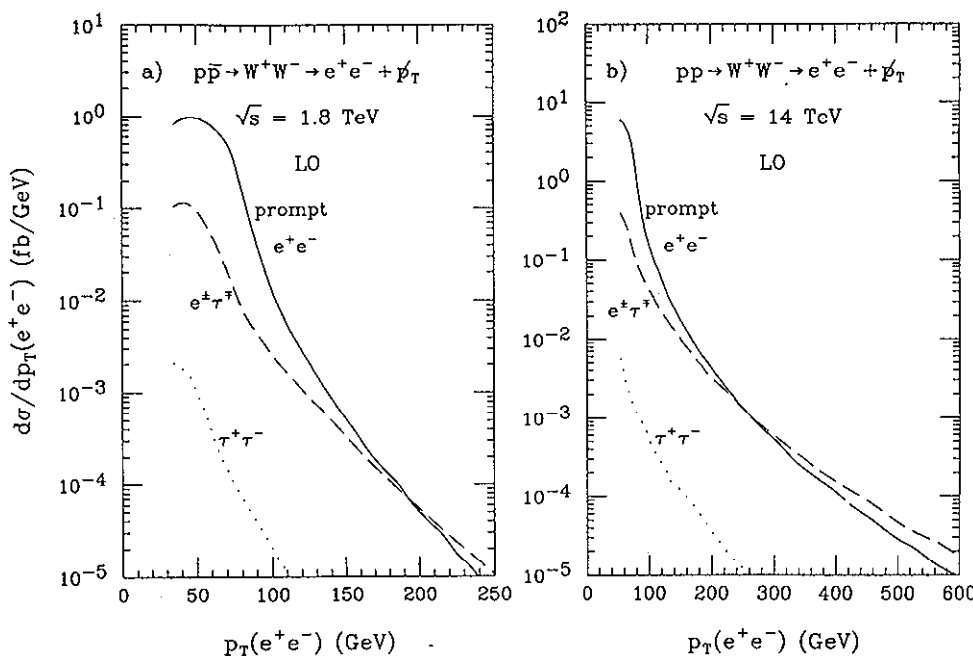

FIG. 12. The LO e^+e^- transverse momentum distribution for (a) $p\bar{p} \rightarrow W^+W^- \rightarrow e^+e^-\not{p}_T$ at $\sqrt{s} = 1.8$ TeV, and (b) $pp \rightarrow W^+W^- \rightarrow e^+e^-\not{p}_T$ at $\sqrt{s} = 14$ TeV. The solid lines show the result for the direct $W \rightarrow e\nu$ decays. The dashed (dotted) lines represent the differential cross sections if one (both) charged lepton(s) in the final state originate, from $W \rightarrow \tau\nu_\tau \rightarrow e\nu_e\nu_\tau\bar{\nu}_\tau$. The cuts imposed are summarized in Sec. III B.

thus slightly reduce the overall sensitivity to anomalous couplings.

G. Sensitivity limits

We now proceed and derive sensitivity limits for anomalous WWV couplings from $W^+W^- + X \rightarrow \ell_1^+ \ell_2^- \not{p}_T + X$, $\ell_{1,2} = e, \mu$, at the Tevatron and LHC. For the Tevatron we consider integrated luminosities of 1 fb^{-1}, as envisioned for the Main Injector Era, and 10 fb^{-1} (TeV*) which could be achieved through additional upgrades of the Tevatron accelerator complex [14]. In the case of the LHC we use $\int \mathcal{L} dt = 10$ fb^{-1} and 100 fb^{-1} [15]. To extract limits, we shall sum over electron and muon final states. Interference effects between different WWV couplings are fully incorporated in our analysis. We derive limits for the cases where either the $WW\gamma$ or the WWZ couplings only are allowed to differ from their SM values, as well as for the HISZ scenario described at the end of Sec. II B. Varying the $WW\gamma$ or WWZ couplings separately makes it possible to directly compare the sensitivity of W^+W^- production to these couplings with that of $W\gamma$ and WZ production. Furthermore, the bounds derived in these limiting cases make it easy to perform a qualitative estimate of sensitivity limits for any model where the WWZ and $WW\gamma$ couplings are related. The HISZ scenario serves as a simple example of such a model. In the form we consider here, only two of the couplings are independent; see Eqs. (9)–(11).

To derive 95% C.L. limits we use the $p_T(\ell_1^+ \ell_2^-)$ distribution and perform a χ^2 test [73], assuming that no deviations from the SM predictions are observed in the experiments considered. As we have seen, the $\ell_1^+ \ell_2^-$ transverse momentum distribution in general yields the best sensitivity bounds in the Born approximation. Furthermore, we impose the cuts summarized in Sec. III B. For simplicity, we do not exclude the region around the Z mass peak in $m(\ell_1^+ \ell_2^-)$ for $\ell_1 = \ell_2$, which is necessary to eliminate the background from $ZZ \rightarrow \ell^+ \ell^- \not{p}_T$. Such a cut does not noticeably influence the high $p_T(\ell_1^+ \ell_2^-)$ region from which most of the sensitivity to anomalous WWV couplings originates. We also ignore any contributions from decay modes where one or both W's decay into a τ lepton. These modes affect the sensitivity to nonstandard WWV couplings only insignificantly (see Sec. III F). Since most background processes can be removed by standard requirements, such as an isolated charged lepton cut, we concentrate on the $t\bar{t}$ background. For the top quark mass we assume $m_t = 176$ GeV. At the Tevatron with 1 fb^{-1} (10 fb^{-1}) we use a jet-defining p_T threshold of 10 GeV (20 GeV), whereas we take 30 GeV (50 GeV) at the LHC for 10 fb^{-1} (100 fb^{-1}). Unless explicitly stated otherwise, a dipole form factor ($n = 2$) with scale $\Lambda_{FF} = 1$ TeV is assumed. The $p_T(\ell_1^+ \ell_2^-)$ distribution is split into a certain number of bins. The number of bins and the bin width depend on the center-of-mass energy and the integrated luminosity. In each bin the Poisson statistics are approximated by a Gaussian distribution. In order to achieve a sizable counting rate in each bin,

all events above a certain threshold are collected in a single bin. This procedure guarantees that a high statistical significance cannot arise from a single event at large transverse momentum, where the SM predicts, say, only 0.01 events. In order to derive realistic limits we allow for a normalization uncertainty of 50% in the SM cross section. By employing more powerful statistical tools than the simple χ^2 test we performed [74], it may be possible to improve the limits we obtain.

In Figs. 13 and 14, and in Table I, we display sensitivity limits for the case where only the WWZ couplings are allowed to deviate from their SM values. The cross section in each bin is a bilinear function of the anomalous couplings $\Delta\kappa_Z^0$, λ_Z^0, and Δg_1^{Z0}. Studying the correlations in the $\Delta\kappa_Z^0$-λ_Z^0, the $\Delta\kappa_Z^0$-Δg_1^{Z0}, and the Δg_1^{Z0}-λ_Z^0 planes is, therefore, sufficient to fully include all interference effects between the various WWZ couplings. Figure 13 (14) shows 95% C.L. contours in the three planes for the Tevatron (LHC) with 1 fb^{-1} (10 fb^{-1}). Without a jet veto, inclusive NLO corrections and the top quark background together reduce the sensitivity obtained from the LO W^+W^- cross section by about a factor 2 to 5. Imposing a jet veto, the $t\bar{t}$ background and the large QCD corrections at high $\ell_1^+ \ell_2^-$ transverse momenta are essentially eliminated at the Tevatron, and the resulting limits are very similar to those obtained from the LO analysis. At the LHC, the remaining top quark background still has a nonnegligible impact, reducing the limits obtained from the analysis of W^+W^- production at LO by a factor 1.5–2. The bounds extracted from the LO W^+W^- cross section represent the results for the ideal case where all background can be completely removed. The limits obtained without reducing the $t\bar{t}$ background and the NLO QCD corrections, on the other hand, correspond to a "worst case scenario," i.e., the minimal sensitivity to anomalous couplings which one should be able to reach.

More detailed information on how QCD corrections and the top quark background influence the limits which can be achieved on WWZ couplings is provided in Table I. At Tevatron energies, NLO QCD corrections reduce the sensitivity by 5–10%, while for the LHC the bounds obtained from the inclusive NLO W^+W^- cross section are typically a factor 2 worse than those extracted using the LO cross section. A 10% (factor 2) variation in the 95% C.L. limits is roughly equivalent to a factor 1.5 (16) in integrated luminosity needed to compensate for the effect of the NLO corrections. The limits found by imposing a $p_T(h)$ cut and a jet-veto requirement are almost identical at the Tevatron. For LHC energies, the $p_T(h)$ cut yields bounds which are 20–40% weaker than those extracted from the exclusive NLO W^+W^- rate.

Terms in the amplitudes proportional to Δg_1^Z grow like $\sqrt{\hat{s}}/M_W$ while terms multiplying $\Delta\kappa_V$ and λ_V increase with $\hat{s}/M_W^2$. As a result, the limits which can be achieved for Δg_1^Z are significantly weaker than the bounds obtained for $\Delta\kappa_Z$ and λ_Z. Our limits also fully reflect the sign dependence of the differential cross sections for Δg_1^Z and $\Delta\kappa_V$ noted earlier.

Limits for the cases in which the $WW\gamma$ couplings are varied (assuming SM WWZ couplings) and the HISZ sce-

nario are shown in Figs. 15 and 16 and Tables II and III. We only display the limits for the NLO 0 jet case, including the residual $t\bar{t}$ background, in these figures and tables. In Fig. 15 we compare the limits for the three different cases for a fixed integrated luminosity. Because of the smaller overall $WW\gamma$ and photon fermion couplings, the bounds on $\Delta\kappa_\gamma$ and λ_γ are about a factor 1.5 to 3 weaker than the limits obtained for WWZ couplings. As a result of the assumed relations between the $WW\gamma$ and

WWZ couplings [see Eqs. (9)–(11)], we find limits on λ_γ ($\Delta\kappa_\gamma$) in the HISZ scenario, which are somewhat better (worse) than those obtained for λ_Z ($\Delta\kappa_Z$) when only the WWZ couplings are varied. The CDF and D0 Collaborations have derived 95% C.L. limit contours for the WWV couplings from W^+W^- production [9,10] for the case $\Delta\kappa_Z = \Delta\kappa_\gamma$, $\lambda_Z = \lambda_\gamma$, and $\Delta g_1^Z = 0$. In this scenario, we find limits which are about 20–40% better than those obtained for the case where only $\Delta\kappa_Z$ and λ_Z are
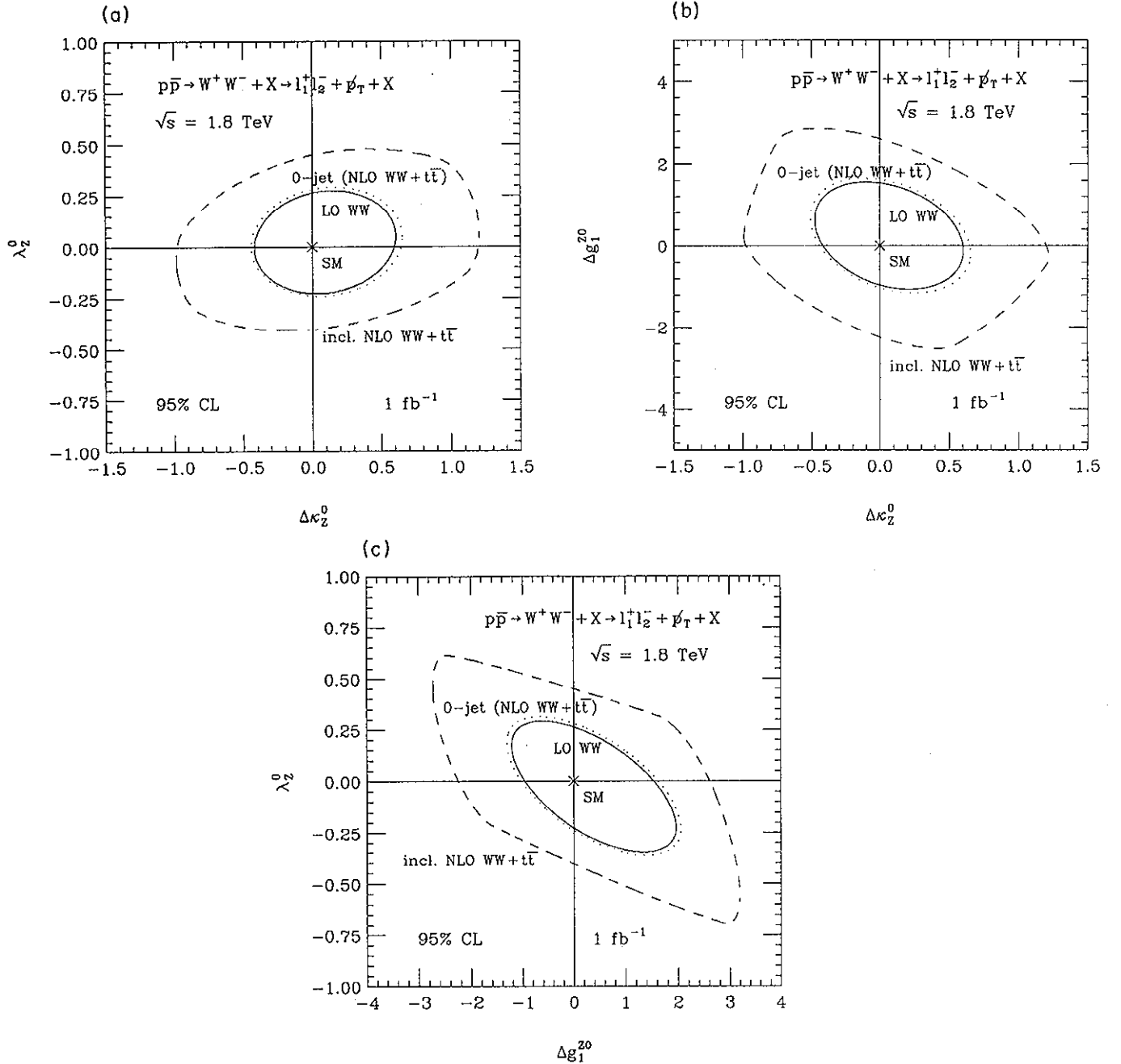

FIG. 13. Limit contours at the 95% C.L. for $p\bar{p} \to W^+W^- + X \to \ell_1^+\ell_2^-\displaystyle{\not}p_T + X$, $\ell_{1,2} = e,\ \mu$, derived from the $p_T(\ell_1^+\ell_2^-)$ distribution at the Tevatron for $\int \mathcal{L}dt = 1$ fb^{-1}. Contours are shown in three planes: (a) the $\Delta\kappa_Z^0$-λ_Z^0 plane, (b) the $\Delta\kappa_Z^0$-Δg_1^{Z0} plane, and (c) the Δg_1^{Z0}-λ_Z^0 plane. The solid lines give the results for LO W^+W^- production, ignoring the $t\bar{t}$ background. The dashed lines show the limits which are obtained if the top quark background is taken into account and the inclusive NLO W^+W^- cross section is used. The dotted lines display the bounds which are achieved from the exclusive NLO $W^+W^- + 0$ jet channel, including the residual $t\bar{t} \to W^+W^- + 0$ jet background. The cuts imposed are summarized in Sec. III B. For the top quark mass we assume $m_t = 176$ GeV, and for the jet definition, we have used Eq. (12).

allowed to deviate from their SM values.

In Fig. 16 we compare the bounds which can be achieved for the HISZ scenario for different integrated luminosities and form factor scales. Increasing the integrated luminosity by one order of magnitude improves the sensitivity limits by a factor 2.0–2.7 at the Tevatron, and up to a factor of 1.8 at the LHC for the form factor scale chosen. Because of the significantly higher residual top quark background, the sensitivity limits which can be achieved at the LHC with 10 fb^{-1} are only up to a factor 2 better than those found at the Tevatron for the same integrated luminosity and form factor scale.

At Tevatron energies, the sensitivities achievable are insensitive to the exact form and scale of the form factor for $\Lambda_{FF} > 400$ GeV. At the LHC, the situation is somewhat different and the sensitivity bounds depend on the value chosen for Λ_{FF}. This is illustrated in Fig. 16(b) and Table III, where we display the limits which can be achieved at the LHC with $\int \mathcal{L}dt = 100$ fb^{-1} and a form factor scale of $\Lambda_{FF} = 3$ TeV. The limits for the

higher scale are a factor 2.8 to 5 better than those found for $\Lambda_{FF} = 1$ TeV with the same integrated luminosity. For $\Lambda_{FF} > 3$ TeV, the sensitivity bounds depend only marginally on the form factor scale [22], due to the very rapidly falling cross section at the LHC for parton center-of-mass energies in the multi-TeV region. The dependence of the limits on the cutoff scale Λ_{FF} in the form factor can be understood easily from Fig. 5. The improvement in sensitivity with increasing Λ_{FF} is because of the additional events at large $p_T(\ell_1^+ \ell_2^-)$ which are suppressed by the form factor if the scale Λ_{FF} has a smaller value.

To a lesser degree, the bounds also depend on the power n in the form factor, which we have assumed to be $n = 2$. For example, the less drastic cutoff for $n = 1$ instead of $n = 2$ in the form factor allows for additional high $p_T(\ell_1^+ \ell_2^-)$ events and therefore leads to a slightly increased sensitivity to the low energy values of the anomalous WWV couplings. The sensitivity bounds listed in Tables I–III can thus be taken as representative for a

TABLE I. Sensitivities achievable at the 95% confidence level (C.L.) for the anomalous WWZ couplings Δg_1^{Z0}, $\Delta \kappa_Z^0$, and λ_Z^0; (a) in $p\bar{p} \rightarrow W^+W^- + X \rightarrow \ell_1^+\ell_2^-\not{p}_T + X$, $\ell_{1,2} = e, \mu$, at the Tevatron ($\sqrt{s} = 1.8$ TeV) with $\int \mathcal{L}dt = 1$ fb^{-1}, and (b) in $pp \rightarrow W^+W^- + X \rightarrow \ell_1^+\ell_2^-\not{p}_T + X$ at the LHC ($\sqrt{s} = 14$ TeV) with $\int \mathcal{L}dt = 10$ fb^{-1}. The limits for each coupling apply for arbitrary values of the two other couplings. The $WW\gamma$ couplings are assumed to take their SM values. For the form factor we use the form of Eq. (8) with $n = 2$ and $\Lambda_{FF} = 1$ TeV. The transverse momentum threshold for the jet veto and the $p_T(h)$ cut is taken to be 10 GeV at the Tevatron, and 30 GeV at the LHC. The $t\bar{t}$ cross section is calculated at LO with $m_t = 176$ GeV. The cuts summarized in Sec. III B are imposed.

(a) Tevatron, $\int \mathcal{L}dt = 1$ fb^{-1}					
	W^+W^-	W^+W^-	$W^+W^- + t\bar{t}$	$W^+W^- + t\bar{t}$	$W^+W^- + t\bar{t}$
WWZ coupling	LO	NLO incl.	NLO incl.	NLO 0 jet	NLO $p_T(h)$ cut
Δg_1^{Z0}	+1.96 −1.22	+2.10 −1.38	+3.19 −2.73	+2.05 −1.31	+2.08 −1.34
$\Delta \kappa_Z^0$	+0.61 −0.48	+0.66 −0.51	+1.22 −0.99	+0.66 −0.51	+0.66 −0.52
λ_Z^0	+0.29 −0.35	+0.32 −0.37	+0.61 −0.70	+0.32 −0.36	+0.32 −0.37

(b) LHC, $\int \mathcal{L}dt = 10$ fb^{-1}					
	W^+W^-	W^+W^-	$W^+W^- + t\bar{t}$	$W^+W^- + t\bar{t}$	$W^+W^- + t\bar{t}$
WWZ coupling	LO	NLO incl.	NLO incl.	NLO 0 jet	NLO $p_T(h)$ cut
Δg_1^{Z0}	+0.55 −0.27	+0.56 −0.61	+1.19 −1.57	+0.81 −0.50	+0.95 −0.68
$\Delta \kappa_Z^0$	+0.129 −0.067	+0.207 −0.129	+0.364 −0.291	+0.187 −0.123	+0.217 −0.156
λ_Z^0	+0.043 −0.045	+0.078 −0.090	+0.138 −0.146	+0.063 −0.071	+0.076 −0.084

wide class of form factors.

As we have mentioned before, constant anomalous couplings are assumed in models based on chiral perturbation theory [38]. Since the sensitivity bounds we obtain at Tevatron energies only marginally depend on Λ_{FF}, they are directly applicable to those models. It is straightforward to convert the anomalous couplings $\Delta\kappa_V$, λ_V, and Δg_1^Z into the parameters generally used in models based on chiral perturbation theory [28].

From our studies we conclude that at the TeV* the WWV couplings can be probed with an accuracy of 10–60%, except for Δg_1^Z. At the LHC, with $\int \mathcal{L} dt = 100$ fb^{-1}, $\Delta\kappa_V^0$ and λ_V^0 can be determined with an uncertainty of a few percent, whereas Δg_1^{Z0} can be measured to approximately 0.2, with details depending on the form factor scale assumed. For a top quark mass of $m_t = 200$ GeV, we find sensitivity bounds which are slightly better than those shown in Figs. 13–16 and Ta-

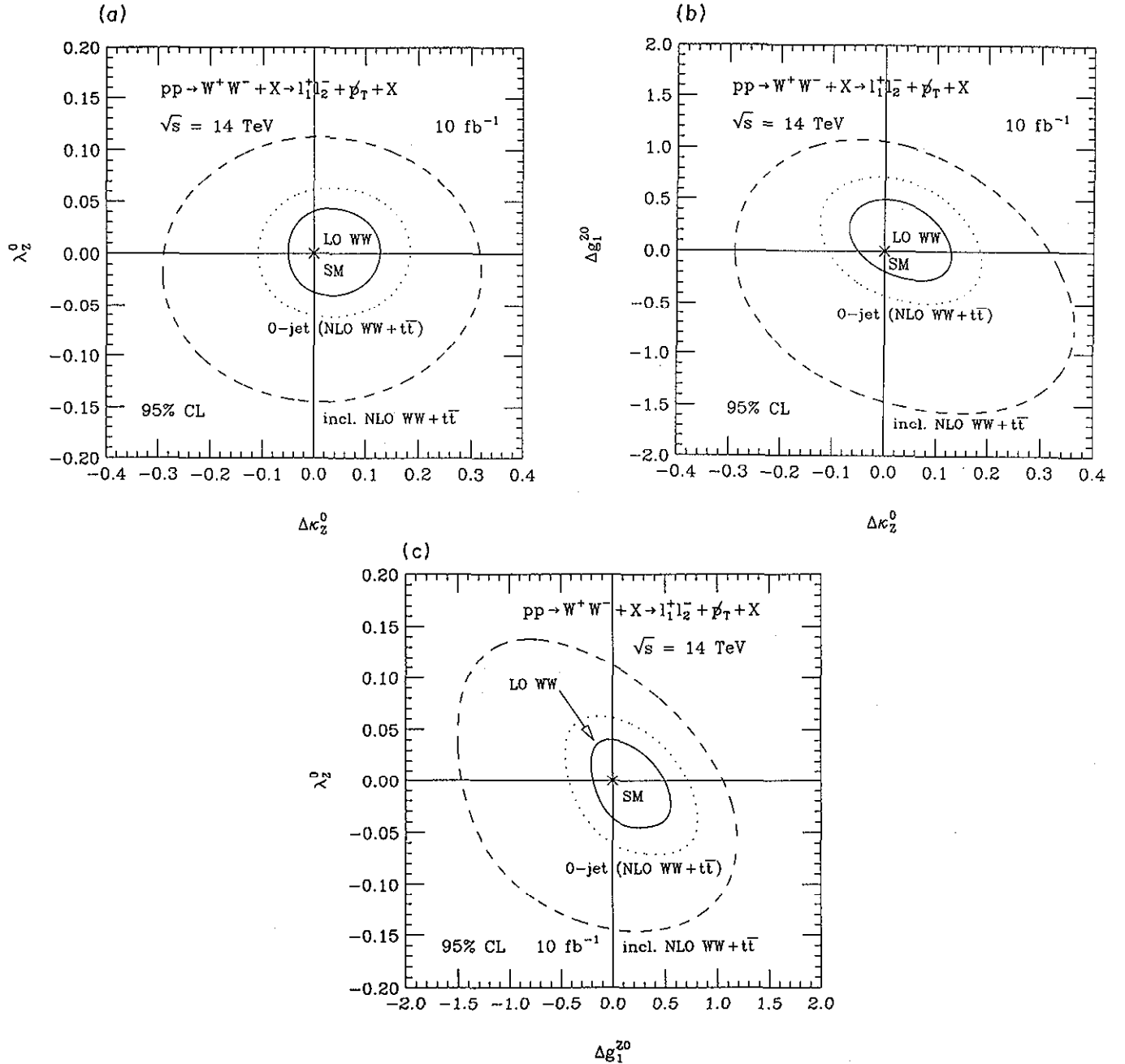FIG. 14. Limit contours at the 95% C.L. for $pp \to W^+W^- + X \to \ell_1^+\ell_2^- \not{p}_T + X$, $\ell_{1,2} = e, \mu$, derived from the $p_T(\ell_1^+\ell_2^-)$ distribution at the LHC for $\int \mathcal{L} dt = 10$ fb^{-1}. Contours are shown in three planes: (a) the $\Delta\kappa_Z^0$-λ_Z^0 plane, (b) the $\Delta\kappa_Z^0$-Δg_1^{Z0} plane, and (c) the Δg_1^{Z0}-λ_Z^0 plane. The solid lines give the results for LO W^+W^- production, ignoring the $t\bar{t}$ background. The dashed lines show the limits which are obtained if the top quark background is taken into account and the inclusive NLO W^+W^- cross section is used. The dotted lines display the bounds which are achieved from the exclusive NLO $W^+W^- + 0$ jet channel, including the residual $t\bar{t} \to W^+W^- + 0$ jet background. The cuts imposed are summarized in Sec. III B. For the top quark mass we assume $m_t = 176$ GeV, and for the jet definition, we have used Eq. (13).

TABLE II. Sensitivities achievable at the 95% confidence level (C.L.) for anomalous WWV couplings ($V = \gamma, Z$) in $p\bar{p} \to W^+W^- + 0$ jet $\to \ell_1^+\ell_2^- \not{p}_T + 0$ jet, $\ell_{1,2} = e, \mu$, at NLO for the Tevatron: (a) for $\int \mathcal{L}dt = 1$ fb^{-1} and (b) for $\int \mathcal{L}dt = 10$ fb^{-1}, including the residual background from $t\bar{t}$ production. Limits are shown for the case where only the $WW\gamma$ or WWZ couplings are allowed to deviate from their SM values, and for the HISZ scenario where we assume $\Delta\kappa_\gamma$ and λ_γ as the independent couplings [see Eqs. (9)–(11)]. Interference effects between those couplings which are varied are fully taken into account. For the form factors we use the form of Eq. (8) with $n = 2$ and $\Lambda_{FF} = 1$ TeV. The transverse momentum threshold for the jet veto and the $p_T(h)$ cut is taken to be 10 GeV for $\int \mathcal{L}dt = 1$ fb^{-1}, and 20 GeV for 10 fb^{-1}. The $t\bar{t}$ cross section is calculated at LO with $m_t = 176$ GeV. The cuts summarized in Sec. III B are imposed.

(a) Tevatron, $\int \mathcal{L}dt = 1$ fb^{-1}			
Coupling	$WW\gamma$	WWZ	HISZ scenario
Δg_1^{Z0}	–	$+2.05$ / -1.31	–
$\Delta\kappa_V^0$	$+1.30$ / -0.92	$+0.66$ / -0.51	$+0.85$ / -0.51
λ_V^0	$+0.58$ / -0.51	$+0.32$ / -0.36	$+0.22$ / -0.20

(b) Tevatron, $\int \mathcal{L}dt = 10$ fb^{-1}			
Coupling	$WW\gamma$	WWZ	HISZ scenario
Δg_1^{Z0}	–	$+1.00$ / -0.53	–
$\Delta\kappa_V^0$	$+0.64$ / -0.35	$+0.32$ / -0.22	$+0.43$ / -0.19
λ_V^0	$+0.25$ / -0.20	$+0.13$ / -0.14	$+0.096$ / -0.086

bles I–III. Limits derived from the transverse momentum distribution of the individual charged leptons are weaker by approximately a factor 1.5 than those extracted from the $p_T(\ell_1^+\ell_2^-)$ spectrum. We have not studied in detail the sensitivities which can be achieved in the current Tevatron collider. For an integrated luminosity of about 100 pb^{-1} the limits which one can hope to achieve are approximately a factor 2 to 3 worse than those found for 1 fb^{-1}.

The results shown in Figs. 13–16 and Tables I–III should be compared with the sensitivities expected in other channels [22,54,59], and in W pair production at

TABLE III. Sensitivities achievable at the 95% confidence level (C.L.) for anomalous WWV couplings ($V = \gamma, Z$) in $pp \to W^+W^- + 0$ jet $\to \ell_1^+\ell_2^- \not{p}_T + 0$ jet, $\ell_{1,2} = e, \mu$, at NLO for the LHC, including the residual background from $t\bar{t}$ production. Limits are shown for the case where only the $WW\gamma$ or WWZ couplings are allowed to deviate from their SM values, and for HISZ scenario where we assume $\Delta\kappa_\gamma$ and λ_γ as the independent couplings [see Eqs. (9)–(11)]. Interference effects between those couplings which are varied are fully taken into account. For the form factors we use the form of Eq. (8) with $n = 2$. The transverse momentum threshold for the jet veto and the $p_T(h)$ cut is taken to be 30 GeV for $\int \mathcal{L}dt = 10$ fb^{-1}, and 50 GeV for 100 fb^{-1}. The $t\bar{t}$ cross section is calculated at LO with $m_t = 176$ GeV. The cuts summarized in Sec. III B are imposed.

(a) LHC, $\int \mathcal{L}dt = 10$ fb^{-1}, $\Lambda_{FF} = 1$ TeV			
Coupling	$WW\gamma$	WWZ	HISZ scenario
Δg_1^{Z0}	–	$+0.81$ / -0.50	–
$\Delta\kappa_V^0$	$+0.43$ / -0.25	$+0.19$ / -0.12	$+0.27$ / -0.14
λ_V^0	$+0.15$ / -0.14	$+0.063$ / -0.071	$+0.052$ / -0.049

(b) LHC, $\int \mathcal{L}dt = 100$ fb^{-1}, $\Lambda_{FF} = 1$ TeV (3 TeV)			
Coupling	$WW\gamma$	WWZ	HISZ scenario
Δg_1^{Z0}	– (–)	$+0.62$ / -0.50 ($+0.22$ / -0.17)	– (–)
$\Delta\kappa_V^0$	$+0.31$ / -0.18 ($+0.067$ / -0.040)	$+0.133$ / -0.085 ($+0.027$ / -0.018)	$+0.201S$ / -0.110 ($+0.047$ / -0.025)
λ_V^0	$+0.092$ / -0.086 ($+0.022$ / -0.022)	$+0.042$ / -0.040 ($+0.0084$ / -0.0111)	$+0.029$ / -0.036 ($+0.0078$ / -0.0079)

LEP II [22,44,75], and a linear e^+e^- collider [76]. The limits which we obtain for the $WW\gamma$ couplings at the Tevatron, assuming a SM WWZ vertex function, are a factor 1.7–4.4 weaker than those projected from $W^\pm\gamma$
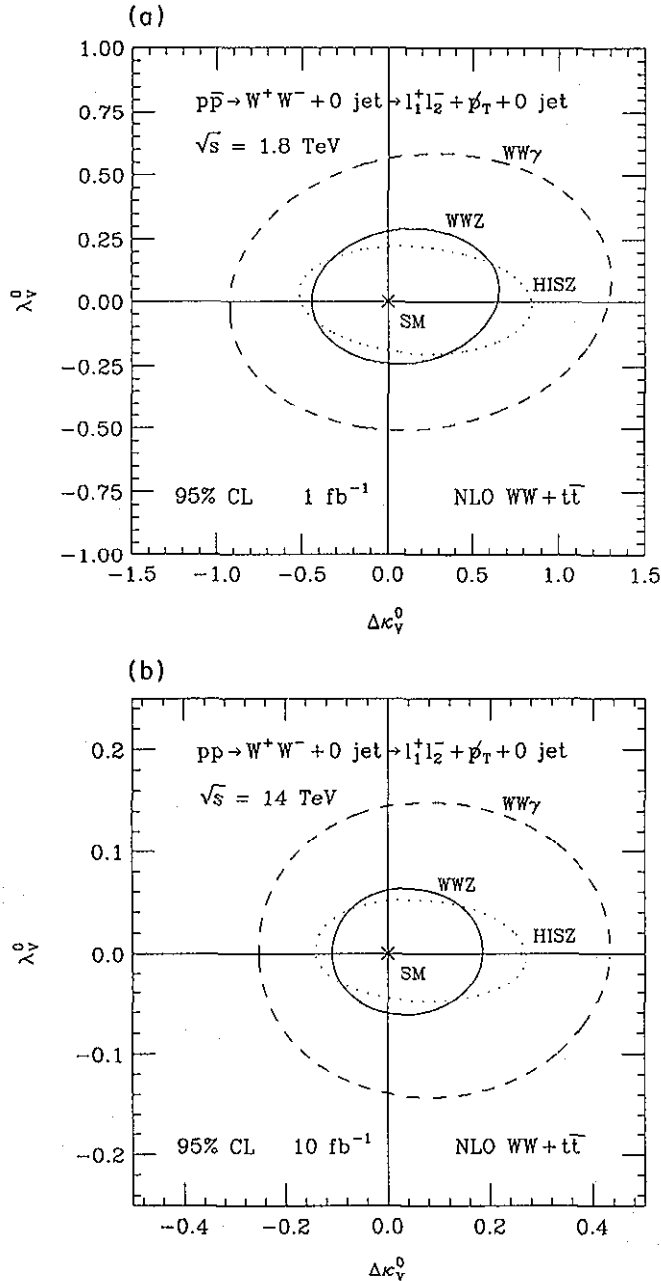

FIG. 15. Limit contours at the 95% C.L. derived from the NLO $p_T(\ell_1^+\ell_2^-)$, $\ell_{1,2} = e, \mu$, distribution for (a) $p\bar{p} \to W^+W^- + 0$ jet $\to \ell_1^+\ell_2^- \not{p}_T + 0$ jet at $\sqrt{s} = 1.8$ TeV with $\int \mathcal{L}dt = 1$ fb^{-1}, and (b) $pp \to W^+W^- + 0$ jet $\to \ell_1^+\ell_2^- \not{p}_T + 0$ jet at $\sqrt{s} = 14$ TeV with $\int \mathcal{L}dt = 10$ fb^{-1} in the $\Delta\kappa_V^0$-λ_V^0 plane. The solid line displays the limits which are achieved if $\Delta\kappa_Z^0$ and λ_Z^0 only are allowed to deviate from their SM values. The dotted and dashed lines show the results obtained in the HISZ scenario [see Eqs. (9)–(11)] and by varying the $WW\gamma$ couplings only. The effect of the residual $t\bar{t} \to e^+e^- \not{p}_T + 0$ jet background is included in the contours shown. The cuts imposed are summarized in Sec. III B. For the top quark mass we assume $m_t = 176$ GeV, and for the jet definition, we have used Eqs. (12) and (13).

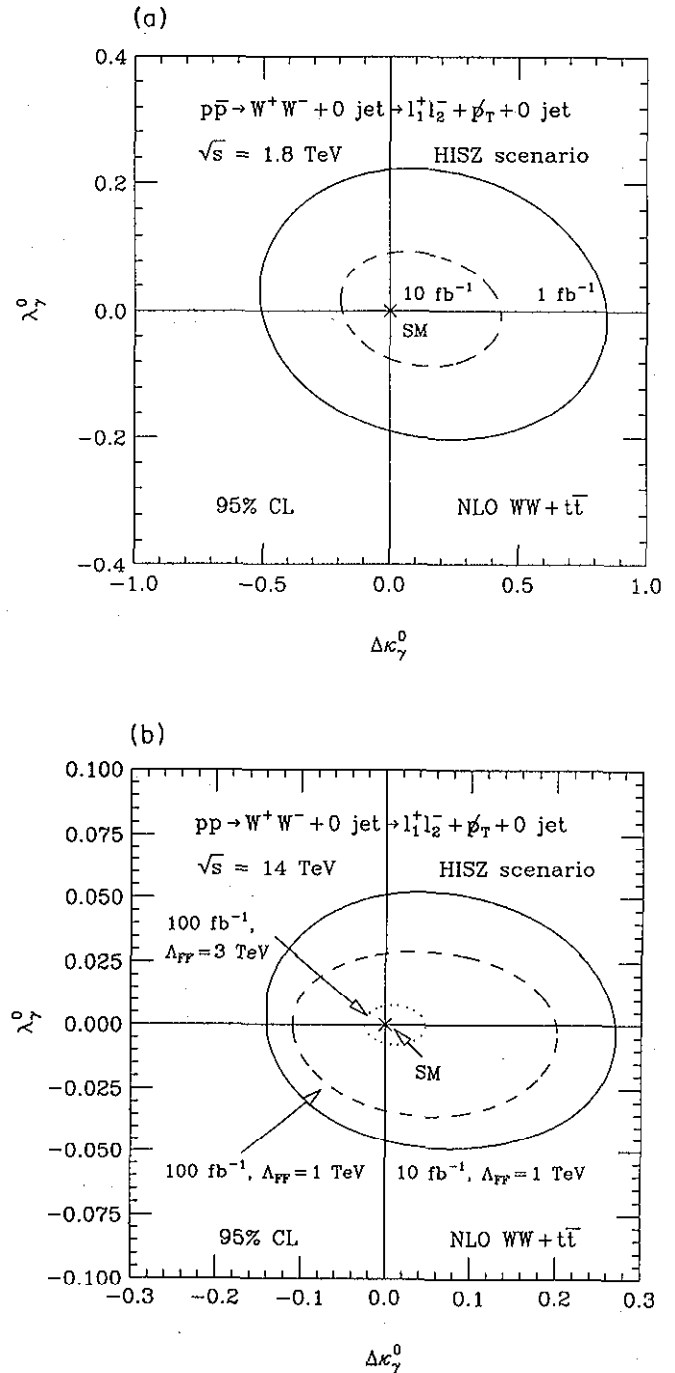FIG. 16. Limit contours at the 95% C.L. derived from the NLO $p_T(\ell_1^+\ell_2^-)$, $\ell_{1,2} = e, \mu$, distribution for (a) $p\bar{p} \to W^+W^- + 0$ jet $\to \ell_1^+\ell_2^- \not{p}_T + 0$ jet at $\sqrt{s} = 1.8$ TeV, and (b) $pp \to W^+W^- + 0$ jet $\to \ell_1^+\ell_2^- \not{p}_T + 0$ jet at $\sqrt{s} = 14$ TeV in the HISZ scenario [see Eqs. (9)–(11)]. In part (a) the solid and dashed lines give the limits for integrated luminosities of $\int \mathcal{L}dt = 1$ fb^{-1} and 10 fb^{-1}, respectively. The form factor scale in both cases is $\Lambda_{FF} = 1$ TeV. In part (b) results are displayed for $\int \mathcal{L}dt = 10$ fb^{-1} (solid curve) and $\int \mathcal{L}dt = 100$ fb^{-1} (dashed curve) with $\Lambda_{FF} = 1$ TeV, and for $\int \mathcal{L}dt = 100$ fb^{-1} with $\Lambda_{FF} = 3$ TeV (dotted curve). The effect of the residual $t\bar{t} \to e^+e^- \not{p}_T + 0$ jet background is included in the contours shown. The cuts imposed are summarized in Sec. III B. For the top quark mass we assume $m_t = 176$ GeV. The jet definition criteria are described in Sec. III E.

production with $W \to e\nu$ [22], mostly because of the smaller event rate. At the LHC, with 100 fb^{-1} and $\Lambda_{\mathrm{FF}} = 3$ TeV, the limits on $\Delta\kappa_\gamma^0$ (λ_γ^0) are a factor 1.5 to 2 (~ 3) better (worse) than those expected from $W\gamma$ production [22,54]. The higher sensitivity of W pair production to $\Delta\kappa_\gamma$ can be traced to the high energy behavior of the terms proportional to $\Delta\kappa_V$ in the helicity amplitudes. As mentioned in the Introduction, these terms increase proportional to $\hat{s}/M_W^2$ in W^+W^- production, whereas they grow only like $\sqrt{\hat{s}}/M_W$ in $p\overset{(-)}{p} \to W^\pm\gamma$, $W^\pm Z$.

The bounds we obtain for the WWZ couplings, assuming a SM $WW\gamma$ vertex, can be compared directly with the sensitivity limits calculated for $W^\pm Z \to \ell_1^\pm\nu_1\ell_2^+\ell_2^-$ in Ref. [59]. The bounds for λ_Z from W^+W^- and $W^\pm Z$ production are very similar. At the LHC, the larger cross section for W^+W^- production is compensated by the considerable top quark background which remains even after a jet veto has been imposed. For Tevatron (LHC) energies, the sensitivity limits for $\Delta\kappa_Z$ from W pair production are approximately a factor 3 (2–7) better than those which can be achieved in $p\bar{p} \to WZ$ $(pp \to WZ)$, whereas the bounds for Δg_1^Z from WZ productions are 3–4 (7–34) times more stringent than those extracted from the W^+W^- channel for the parameters chosen. WW and WZ productions at hadron colliders thus yield complementary information on Δg_1^Z and $\Delta\kappa_Z$. The limits fully reflect the high energy behavior of the individual helicity amplitudes for the two processes. Terms proportional to λ_Z increase in both cases like $\hat{s}/M_W^2$. On the other hand, the leading Δg_1^Z $(\Delta\kappa_Z)$ terms in WZ (WW) production grow faster with energy [$\sim \hat{s}/M_W^2$] than those in the WW (WZ) production [$\sim \sqrt{\hat{s}}/M_W$].

In the HISZ scenario, WW production leads to bounds for $\Delta\kappa_\gamma$ which, at the Tevatron (LHC), are up to factor of 2 (5) weaker than those obtained in $W\gamma$ and WZ production [22]. The limits on λ_γ from W pair production at the Tevatron (LHC) in this model are slightly better (worse) than those derived from $W^\pm Z \to \ell_1^\pm\nu_1\ell_2^+\ell_2^-$.

As has been demonstrated by the CDF Collaboration [9], useful limits on the WWV couplings can also be derived from WW, $WZ \to \ell\nu jj$, and $WZ \to \ell^+\ell^- jj$ at large dijet transverse momenta, $p_T(jj)$. Decay modes, where one of the vector bosons decays hadronically, have a considerably larger branching ratio than the $W^+W^- \to \ell_1^+\nu_1\ell_2^-\bar{\nu}_2$ channel and thus yield higher rates. On the other hand, a jet veto cannot be utilized to reduce the top background for the semihadronic final states. Because of the very large $t\bar{t}$ background at the LHC, decay modes, where one of the vector bosons decays into hadrons, are therefore only useful at Tevatron energies where the total $t\bar{t}$ and W^+W^- production rates are comparable. Here, a sufficiently large $p_T(jj)$ cut eliminates the QCD $W/Z+$ jets background and the SM signal, but retains good sensitivity to anomalous WWV couplings. The value of the $p_T(jj)$ cut varies with the integrated luminosity assumed. Simulations of the sensitivities which may be expected in the HISZ scenario for WW, $WZ \to \ell\nu jj$, and $WZ \to \ell^+\ell^- jj$ in future Tevatron experiments show [22] that, for 1 fb^{-1}, the semihadronic final states yield bounds for $\Delta\kappa_\gamma$ which

are roughly a factor of 2 more stringent as those from $W^+W^- \to \ell_1^+\nu_1\ell_2^-\bar{\nu}_2$, whereas the limits on λ_γ are very similar. With growing integrated luminosity, it is necessary to raise the $p_T(jj)$ cut to eliminate the $W/Z+$ jets background. For increasing values of $p_T(jj)$, more and more jets tend to coalesce. At $\int \mathcal{L}dt \geq 10$ fb^{-1}, jet coalescing severely degrades the limits on anomalous WWV couplings which can be achieved. With growing integrated luminosity, W^+W^- production in all leptonic channels thus becomes increasingly potent in constraining the WWV vertices.

The sensitivities in the HISZ scenario which one hopes to achieve from $p\bar{p} \to W^+W^- + 0$ jet $\to \ell_1^+\ell_2^-\slashed{p}_T + 0$ jet (short dashed line) and the other di-boson production channels (adopted from Ref. [22]) at the Tevatron with 10 fb^{-1} are summarized in Fig. 17 and compared with the expectations from $e^+e^- \to W^+W^- \to \ell\nu jj$ at LEP II for $\sqrt{s} = 190$ GeV and $\int \mathcal{L}dt = 500$ pb^{-1} (long dashed line) [77]. A similar comparison, with very similar conclusions, can be carried out for the more conservative choices of an integrated luminosity of 1 fb^{-1} at the Tevatron, and a center-of-mass energy of $\sqrt{s} = 176$ GeV at LEP II [77]. While $W\gamma$ production is seen to yield the best bounds at the Tevatron over a large fraction of the parameter space, it is clear that the limits obtained from the various processes are all of similar magnitude. In particular, the limits from all leptonic decays of W pairs are seen to be comparable to those from the other WW and WZ channels for a significant part of the $\Delta\kappa_\gamma^0$-λ_γ^0 plane. Performing a global analysis of all di-boson pro-

limits on anomalous WWV couplings
Tev, 10 fb^{-1} vs. LEP II, $\sqrt{s} = 190$ GeV, 500 pb^{-1}
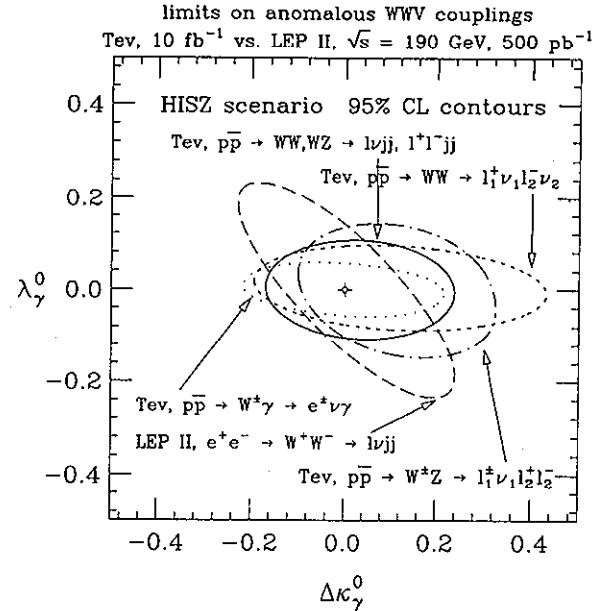
FIG. 17. Comparison of the expected sensitivities on anomalous WWV couplings in the HISZ scenario [see Eqs. (9)–(11)] from $e^+e^- \to W^+W^- \to \ell\nu jj$ at LEP II ($\sqrt{s} = 190$ GeV, $\int \mathcal{L}dt = 500$ pb^{-1}), and di-boson production processes at the Tevatron ($\int \mathcal{L}dt = 10$ fb^{-1}). Except for the short dashed curve, which shows the result for $p\bar{p} \to W^+W^- + 0$ jet $\to \ell_1^+\ell_2^-\slashed{p}_T + 0$ jet at $\sqrt{s} = 1.8$ TeV, all curves are taken from Ref. [22].

duction channels thus is expected to result in a significant improvement of the sensitivity bounds which can be achieved.

Figure 17 also demonstrates that the limits from diboson production at the Tevatron and W^+W^- production at LEP II are quite complementary. The contour for $e^+e^- \rightarrow W^+W^- \rightarrow \ell\nu jj$ in Fig. 17 has been adopted from Ref. [22], and is based on an analysis which takes into account initial state radiation and finite detector resolution effects, together with ambiguities in reconstructing the W decay angles in hadronic W decays in absence of a readily recognizable quark tag. Information on the WWV couplings in $e^+e^- \rightarrow W^+W^- \rightarrow \ell^\pm\nu jj$ is extracted from the angular distribution of the final state fermions. Of the three final states available in W pair production, $\ell_1\nu_1\ell_2\nu_2$, $\ell\nu jj$, $\ell = e$, μ, and $jjjj$, the $\ell\nu jj$ channel yields the best sensitivity bounds. The purely leptonic channel is plagued by a small branching ratio ($\approx 4.7\%$) and by reconstruction problems because of the presence of two neutrinos. In the $jjjj$ final state it is difficult to discriminate the W^+ and W^- decay products. Because of the resulting ambiguities in the $W^\pm$ production and decay angles, the sensitivity bounds which can be achieved from the 4 jet final state are a factor 1.5–2 weaker than those found from analyzing the $\ell\nu jj$ state [75].

At the NLC, the WWV couplings can be tested with a precision of 10^{-3} or better. Details depend quite sensitively on the center-of-mass energy and the integrated luminosity of the NLC [76].

IV. SUMMARY

W^+W^- production in hadronic collisions provides an opportunity to probe the structure of the $WW\gamma$ and WWZ vertices in a direct and essentially model-independent way. In contrast to other diboson production processes at hadron or e^+e^- colliders, the reaction $p\overset{(-)}{p} \rightarrow W^+W^- \rightarrow \ell_1^+\nu_1\ell_2^-\bar{\nu}_2$ offers the possibility to simultaneously probe the high energy behavior and, at least indirectly, the helicity structure of the W^+W^- production amplitudes using the same observable. Usually, information on the high energy behavior of the diboson production amplitudes is obtained from transverse momentum and invariant mass spectra, whereas angular distributions are used to probe the helicity structure [1].

Previous studies of $p\overset{(-)}{p} \rightarrow W^+W^-$ [4–8] have been based on leading-order calculations. In this paper we have presented an $O(\alpha_s)$ calculation of the reaction $p\overset{(-)}{p} \rightarrow W^+W^- + X \rightarrow \ell_1^+\nu_1\ell_2^-\bar{\nu}_2 + X$ for general, C- and P-conserving, $WW\gamma$ and WWZ couplings, using a combination of analytic and Monte Carlo integration techniques. The leptonic decays $W \rightarrow \ell\nu$ have been included in the narrow width approximation in our calculation. Decay spin correlations are correctly taken into account in the calculation, except in the finite virtual contribution. The finite virtual correction term contributes only at the few percent level to the total NLO cross section, thus decay spin correlations can be safely ignored

here. The calculation presented here complements earlier $O(\alpha_s)$ calculations of $W^\pm\gamma$ [58] and $W^\pm Z$ [59] production at hadron colliders for general C- and P-conserving anomalous WWV couplings ($V = \gamma, Z$).

In the past, all leptonic W^+W^- decay channels were not considered in detail, because of the large $t\bar{t}$ background and event reconstruction problems. The presence of two neutrinos in the event makes it impossible to reconstruct the WW invariant mass or the W transverse momentum distribution. We have found that the limited information available for the final state does not reduce the sensitivity to anomalous couplings seriously when the transverse momentum distribution of the charged lepton pair, or equivalently, the missing p_T distribution, is considered. In contrast with other distributions, the lepton pair transverse momentum $p_T(\ell_1^+\ell_2^-)$ distribution is not only sensitive to the high energy behavior of the W^+W^- production amplitudes, but also provides indirect information on the helicities of the W bosons, which are strongly correlated in W pair production in the SM [1,5,17] (see Sec. III C). The correlation of the weak boson helicities, together with the $V - A$ structure of the $We\nu$ coupling and the $2 \rightarrow 2$ kinematics of leading-order W pair production, causes a tendency for the transverse momentum vectors of the two charged leptons to cancel, with a corresponding sharp drop in the leading-order SM $p_T(\ell_1^+\ell_2^-)$ distribution at high transverse momenta. Anomalous WWV couplings do not only change the high energy behavior of the helicity amplitudes, but also modify the correlation of the W helicities. As a result, the $p_T(\ell_1^+\ell_2^-)$ distribution, at leading-order, exhibits a particularly pronounced sensitivity to nonstandard WWV couplings. Decay channels, where one of the final state charged leptons originates from $W \rightarrow \tau\nu_\tau \rightarrow \ell\nu_\ell\nu_\tau\bar{\nu}_\tau$, slightly modify the shape of the $p_T(\ell_1^+\ell_2^-)$ distribution (see Sec. III F).

The real emission processes, $q\bar{q} \rightarrow W^+W^-g$ and $qg \rightarrow W^+W^-q$, which contribute to the $O(\alpha_s)$ QCD corrections in W pair production, spoil the delicate balance of the charged lepton transverse momenta. As a result, inclusive NLO QCD corrections to the $p_T(\ell_1^+\ell_2^-)$ and $\not{p}_T$ distributions are very large and may drastically reduce the sensitivity to nonstandard WWV couplings. By imposing a jet veto, i.e., by considering the exclusive $W^+W^- + 0$ jet channel instead of inclusive $W^+W^- + X$ production, the QCD corrections are reduced to approximately 20% of the LO cross section, and the sensitivity to nonstandard WWV couplings is largely restored. Furthermore, the dependence of the NLO $W^+W^- + 0$ jet cross section on the factorization scale Q^2 is significantly reduced compared to that of the inclusive NLO $W^+W^- + X$ cross section. Uncertainties which originate from the variation of Q^2 will thus be smaller for sensitivity bounds obtained from the $W^+W^- + 0$ jet channel than for those derived from the inclusive NLO $W^+W^- + X$ cross section.

A jet veto, or a cut on the hadronic transverse momentum, $p_T(h)$, also helps to control the $t\bar{t}$ background. Without imposing such a cut, the top quark background is much larger than the W^+W^- signal at high $\ell_1^+\ell_2^-$

transverse momenta and one looses by a factor 2 to 5 in sensitivity. The jet veto in general is more efficient than a $p_T(h)$ cut in reducing the top quark background (see Fig. 10). In practice, this difference is not very important. For realistic $p_T(j)$ and $p_T(h)$ thresholds, the $t\bar{t}$ background can be almost completely eliminated at Tevatron energies. At the LHC, for both methods only a signal to background ratio of order 1 can be achieved. The residual $t\bar{t}$ background weakens the sensitivity bounds on anomalous couplings by about a factor 1.5–2. Overall, the improvement of the sensitivity bounds resulting from a jet veto or a cut on the hadronic transverse momentum is equivalent to roughly a factor 10–40 increase in integrated luminosity.

Excluding the region around the Z mass in $m(\ell_1^+\ell_2^-)$ for $\ell_1 = \ell_2$ eliminates the $ZZ \to \ell^+\ell^-\not{p}_T$ background which otherwise dominates over the W^+W^- signal at large values of $p_T(\ell_1^+\ell_2^-)$. This cut has almost no effect on the high $\ell_1^+\ell_2^-$ transverse momentum tail.

Because of the larger coupling of the Z boson to quarks and W bosons, W^+W^- production is more sensitive to WWZ couplings than $WW\gamma$ couplings. Terms proportional to $\Delta\kappa_V$ in the amplitude grow like $\hat{s}/M_W^2$, where $\hat{s}$ is the parton center-of-mass energy squared, whereas these terms only grow like $\sqrt{\hat{s}}/M_W$ in $W^\pm\gamma$ and $W^\pm Z$ production. W^+W^- production therefore is considerably more sensitive to $\Delta\kappa_V$ than $p\overset{(-)}{p} \to W^\pm\gamma$, $W^\pm Z$. For example, at the Tevatron (LHC) with $\int \mathcal{L}dt = 10$ fb^{-1} (100 fb^{-1}), varying only the WWZ couplings, $\Delta\kappa_Z^0$ can be measured with 20–30% (up to 2–3%) accuracy [95% C.L.] in W pair production in the purely leptonic channels. These bounds are a factor 2 to 7 better than

those which can be achieved in WZ production. Similarly, W pair production yields better limits for $\Delta\kappa_\gamma$ than for $W^\pm\gamma$ production at the LHC for a form factor scale $\Lambda_{FF} > 2$ TeV, if the $WW\gamma$ couplings only are varied. The sensitivity bounds which can be achieved for $\Delta\kappa_V$ at the LHC approach the level where one would hope to see deviations from the SM if new physics with a scale of $O(1$ TeV$)$ exists. λ_V can be determined with an accuracy of 10–25 % (0.9–9 %) at the Tevatron (LHC), whereas Δg_1^Z can be probed at best at the 50% (20%) level. At the LHC, the limits depend significantly on the form factor scale assumed. Detailed results are shown in Figs. 13–16 and Tables I–III.

In the HISZ scenario [see Eqs. (9)–(11)], W pair production at the Tevatron and LEP II yield 95% C.L. limit contours which are quite complementary (see Fig. 17).

ACKNOWLEDGMENTS

[1] K. Hagiwara, R.D. Peccei, D. Zeppenfeld, and K. Hikasa, Nucl. Phys. **B282**, 253 (1987).

[2] F. Berends and A. van Sighem, Nucl. Phys. **B454**, 467 (1995), and references therein.

[3] B. Flaugher, in Proceedings of the "Les Recontres de Physique de la Vallée d' Aoste," La Thuile, Italy, 1995, Report No. FERMILAB-Conf-95/180-E (unpublished).

[4] R.W. Brown and K.O. Mikaelian, Phys. Rev. D **19**, 922 (1979).

[5] C.L. Bilchak and J. Stroughair, Z. Phys. C **23**, 377 (1984).

[6] M. Kuroda et al., Nucl. Phys. **B284**, 271 (1987); C.-H. Chang and S.-C. Lee, Phys. Rev. D **37**, 101 (1988).

[7] K. Hagiwara, J. Woodside, and D. Zeppenfeld, Phys. Rev. D **41**, 2113 (1990).

[8] E. Eichten, I. Hinchliffe, K. Lane, and C. Quigg, Rev. Mod. Phys. **56**, 579 (1984); **58**, 1065(E) (1986).

[9] CDF Collaboration, F. Abe et al., Phys. Rev. Lett. **75**, 1018 (1995).

[10] D0 Collaboration, S. Abachi et al., Phys. Rev. Lett. **75**, 1024 (1995).

[11] J. Ohnemus, Phys. Rev. D **44**, 1403 (1991).

[12] S. Frixione, Nucl. Phys. **B410**, 280 (1993).

[13] T. Diehl, in the Proceedings of the "10th Topical Workshop on Proton Antiproton Physics," Fermilab, 1995, Report No. FERMILAB-Conf-95/165-E (unpublished).

[14] D. Amidei et al., in The Albuquerque Meeting, Proceedings of the Meeting of the Division of Particles and Fields of the APS, Albuquerque, New Mexico, 1994, edited by S. Seidel (World Scientific, Singapore, 1995), Vol. 2, p. 1451; S. Holmes, G. Dugan, and S. Peggs, in Research Directions for the Decade, Proceedings of the Summer Study, Snowmass, Colorado, 1990, edited by E. L. Berger, (World Scientific, Singapore, 1991), p. 674.

[15] The LHC Study Group, "Design Study of the Large Hadron Collider," Report No. CERN 91-03, 1991 (unpublished); L. R. Evans, in Proceedings of the 27th International Conference on High Energy Physics, Glasgow, Scotland, 1994, edited by P.J. Bussey and I.G. Knowles (IOP, London, 1995), Vol. II, p. 1417; Report NO. CERN-AC-95-002, 1995 (unpublished); C.W. Fabjan, Report No. CERN-PPE/95-25, 1995 (unpublished).

[16] H. Baer, J. Ohnemus, and J.F. Owens, Phys. Rev. D **40**, 2844 (1989); ibid. **42**, 61 (1990); Phys. Lett. B **234**, 127 (1990); J. Ohnemus and J.F. Owens, Phys. Rev. D **43**, 3626 (1991); J. Ohnemus, ibid. **44**, 1403 (1991); **44**, 3477 (1991); H. Baer and M.H. Reno, ibid. **43**, 2892 (1991); B. Bailey, J. Ohnemus, and J.F. Owens, ibid. **46**, 2018 (1992); J. Ohnemus, ibid. **47**, 940 (1993); J. Ohnemus and W.J. Stirling, ibid. **47**, 2722 (1993); H. Baer, B. Bai-

ley, and J.F. Owens, *ibid.* **47**, 2730 (1993); L. Bergmann, Ph.D. dissertation, Florida State University, 1989.

[17] C. Bilchak, R. Brown, and J. Stroughair, Phys. Rev. D **29**, 375 (1984).

[18] J. Ohnemus, Phys. Rev. D **50**, 1931 (1994).

[19] U. Baur and D. Zeppenfeld, Phys. Rev. Lett. **75**, 1002 (1995); E.N. Argyres *et al.*, Phys. Lett. B **358**, 339 (1995); C. Papadopoulos, Phys. Lett. B **352**, 144 (1995); J. Papavassiliou and A. Pilaftsis, Phys. Rev. Lett. **75**, 3060 (1995); Report No. NYU-TH/95-03, 1995 (unpublished); G. Lopez Castro, J.L.M. Lucio, and J. Pestieau, Mod. Phys. Lett. A **6**, 3679 (1991); Report No. hep-ph/9504351, 1995 (unpublished); M. Nowakowski and A. Pilaftsis, Z. Phys. C **60**, 121 (1993); A. Aeppli, F. Cuypers, and G. J. van Oldenborgh, Phys. Lett. B **314**, 413 (1993).

[20] G. 't Hooft and M. Veltman, Nucl. Phys. **B44**, 189 (1972).

[21] U. Baur, E.W.N. Glover, and J.J. van der Bij, Nucl. Phys. **B 318**, 106 (1989); V. Barger, T. Han, J. Ohnemus, and D. Zeppenfeld, Phys. Rev. D **41**, 2782 (1990).

[22] H. Aihara *et al.*, in *Electroweak Symmetry Breaking and New Physics at the Tev Scale*, edited by T. Barklow, S. Dawson, H. Haber, and J. Siegrist (World Scientific, Singapore, in press).

[23] CDF Collaboration, F. Abe *et al.*, Phys. Rev. Lett. **74**, 1936 (1995).

[24] D0 Collaboration, S. Abachi *et al.*, Phys. Rev. Lett. **75**, 1034 (1995).

[25] A. De Rujula *et al.*, Nucl. Phys. **B384**, 31 (1992); P. Hernández and F.J. Vegas, Phys. Lett. B **307**, 116 (1993).

[26] C. Burgess and D. London, Phys. Rev. Lett. **69**, 3428 (1992); Phys. Rev. D **48**, 4337 (1993).

[27] K. Hagiwara, S. Ishihara, R. Szalapski, and D. Zeppenfeld, Phys. Lett. B **283**, 353 (1992); Phys. Rev. D **48**, 2182 (1993).

[28] S. Dawson and G. Valencia, Nucl. Phys. **B439**, 3 (1995).

[29] P. Méry, S.E. Moubarik, M. Perrottet, and F.M. Renard, Z. Phys. C **46**, 229 (1990); C. Arzt, M. Einhorn, and J. Wudka, Phys. Rev. D **49**, 1370 (1994).

[30] S.P. Chia, Phys. Lett. B **240**, 465 (1990); K. Numata, Z. Phys. C **52**, 691 (1991); K.A. Peterson, Phys. Lett. B **282**, 207 (1992); T.G. Rizzo, *ibid.* **315**, 471 (1993); U. Baur, in *Proceedings of the Workshop on B Physics at Hadron Accelerators*, Snowmass, Colorado, 1993, edited by C. Shekhar Mishra and P. McBride (Fermilab, Batavia, 1994), p. 455; X. He and B. McKellar, Phys. Lett. B **320**, 165 (1994); R. Martinez, M.A. Pérez, and J.J. Toscano, *ibid.* **340**, 91 (1994).

[31] CLEO Collaboration, M. S. Alam *et al.*, Phys. Rev. Lett. **74**, 2885 (1995).

[32] X. He, Phys. Lett. B **319**, 327 (1993).

[33] G. Baillie, Z. Phys. C **61**, 667 (1994).

[34] X. He and B. McKellar, Phys. Rev. D **51**, 6484 (1995).

[35] G. Belanger, F. Boudjema, and D. London, Phys. Rev. Lett. **65**, 2943 (1990); O. Eboli *et al.*, Phys. Lett. B **339**, 119 (1994); F. M. Renard and C. Verzegnassi, *ibid.* **345**, 500 (1995).

[36] K. Hagiwara, S. Matsumoto, D. Haidt, and C. S. Kim, Z. Phys. C **64**, 559 (1994); S. Matsumoto, Report No. KEK-TH-418, 1994 (unpublished).

[37] C. Arzt, M.B. Einhorn, and J. Wudka, Nucl. Phys. **B433**, 41 (1994).

[38] A. Falk, M. Luke, and E. Simmons, Nucl. Phys. **B365**, 523 (1991).

[39] J. Bagger, S. Dawson, and G. Valencia, Nucl. Phys. **B399**, 364 (1993); M.J. Herrero and E. Ruiz Morales, *ibid.* **B418**, 431 (1994); J. Wudka, Int. J. Mod. Phys. A **9**, 2301 (1994).

[40] J.A.M. Vermaseren, *FORM User's Manual*, (CAN, Amsterdam, 1989).

[41] J.M. Cornwall, D.N. Levin, and G. Tiktopoulos, Phys. Rev. Lett. **30**, 1268 (1973); Phys. Rev. D **10**, 1145 (1974); C.H. Llewellyn Smith, Phys. Lett. **46B**, 233 (1973); S.D. Joglekar, Ann. Phys. (N.Y.) **83**, 427 (1974).

[42] U. Baur and D. Zeppenfeld, Phys. Lett. B **201**, 383 (1988); Nucl. Phys. **B308**, 127 (1988).

[43] W. Buchmüller and D. Wyler, Nucl. Phys. **B268**, 621 (1986).

[44] M. Bilenky *et al.*, Nucl. Phys. **B409**, 22 (1993), and references therein.

[45] D. Dicus and C. Kao, Phys. Rev. D **43**, 1555 (1991); C. Kao (private communication).

[46] CDF Collaboration, F. Abe *et al.*, Phys. Rev. Lett. **73**, 225 (1994); Phys. Rev. **50**, 2966 (1994); Phys. Rev. Lett. **74**, 2626 (1995); Report No. FERMILAB-Pub-95/149-E, 1995 (unpublished).

[47] D0 Collaboration, S. Abachi *et al.*, Phys. Rev. Lett. **74**, 2422 (1995); **74**, 2632 (1995); Phys. Rev. D **52**, 4877 (1995).

[48] D. Schaile, in *Proceedings of the 27th International Conference on High Energy Physics* [15], Vol. I, p. 27; The LEP Collaboration, Report No. CERN-PPE/94-187, 1994 (unpublished).

[49] SLD Collaboration, K. Abe *et al.*, Phys. Rev. Lett. **73**, 25 (1994).

[50] UA2 Collaboration, J. Alitti *et al.*, Phys. Lett. B **241**, 150 (1990); CDF Collaboration, F. Abe *et al.*, Phys. Rev. Lett. **65**, 2243 (1990); Phys. Rev. D **43**, 2070 (1991); CDF Collaboration, F. Abe *et al.*, Phys. Rev. Lett. **75**, 11 (1995); Phys. Rev. D **52**, 4784 (1995).

[51] W.A. Bardeen, A.J. Buras, D.W. Duke, and T. Muta, Phys. Rev. D **18**, 3998 (1978).

[52] A.D. Martin, R.G. Roberts, and W.J. Stirling, Phys. Rev. D **50**, 6734 (1994).

[53] C. Albajar *et al.*, in *Proceedings of the ECFA Large Hadron Collider Workshop*, Germany, 1990, edited by G. Jareskog and D. Rein (CERN Report No. 90-10, Geneva, Switzerland, 1990), Vol. II, p. 621.

[54] ATLAS Collaboration, D. Gingrich *et al.*, ATLAS Letter of Intent, Report No. CERN-LHCC-92-4, 1992 (unpublished); ATLAS Collaboration, W.W. Armstrong *et al.*, ATLAS Technical Design Report, Report No. CERN-LHCC-94-43, 1994 (unpublished).

[55] CMS Collaboration, M. Della Negra *et al.*, CMS Letter of Intent, Report No. CERN-LHCC-92-3, 1992 (unpublished); CMS Collaboration, G.L. Bayatian *et al.*, CMS Technical Design Report, Report No. CERN-LHCC-94-38, 1994 (unpublished).

[56] CDF Collaboration, F. Abe *et al.*, Phys. Rev. D **45**, 3921 (1992).

[57] S. Frixione, P. Nason, and G. Ridolfi, Nucl. Phys. **B383**, 3 (1992).

[58] U. Baur, T. Han, and J. Ohnemus, Phys. Rev. D **48**, 5140 (1993).

[59] U. Baur, T. Han, and J. Ohnemus, Phys. Rev. D **51**, 3381 (1995).

[60] G. Ciapetti and A. Di Ciaccio, in *Proceedings of the ECFA Workshop on LHC Physics*, Aachen, Germany, 1990, edited by G. Jarlskog and D. Rein (CERN, Geneva), Vol. II, p. 155.

[61] T. Han, R. Meng, and J. Ohnemus, Nucl. Phys. **B384**, 59 (1992); P. Arnold and R. Kauffman, *ibid.* **349**, 381 (1991); R. Kauffman, Phys. Rev. D **44**, 1415 (1991); *ibid.* **45**, 1512 (1992); C.P. Yuan, Phys. Lett. B **283**, 395 (1992).

[62] R. Kleiss and W. J. Stirling, Z. Phys. C **40**, 419 (1988); V. Barger, J. Ohnemus, and R.J.N. Phillips, Int. J. Mod. Phys. A **4**, 617 (1989).

[63] F. Cavanna, D. Denegri, and T. Rodrigo, in *Proceedings of the ECFA Workshop on LHC Physics* [60], Vol. II, p. 329.

[64] G. Ladinsky and C.P. Yuan, Phys. Rev. D **43**, 789 (1991); C.P. Yuan, Report No. MSUHEP-50228, 1995 (unpublished); S. Keller (private communication).

[65] V. Barger and R.J.N. Phillips, Phys. Rev. Lett. **55**, 2752 (1985); H. Baer *et al.*, Phys. Rev. D **37**, 3152 (1988).

[66] S. Willenbrock and D. Dicus, Phys. Rev. D **34**, 155 (1986); C.-P. Yuan, *ibid.* **41**, 42 (1990); R. K. Ellis and S. Parke, *ibid.* **46**, 3785 (1992); D. Carlson and C.-P. Yuan, Phys. Lett. B **306**, 386 (1993); G. Bordes and B. van Eijk, Nucl. Phys. **B435**, 23 (1995).

[67] W. Marciano, A. Stange, and S. Willenbrock, Phys. Rev. D **50**, 4491 (1994).

[68] S. Cortese and R. Petronzio, Phys. Lett. B **253**, 494 (1991); T. Stelzer and S. Willenbrock, *ibid.* **357**, 125 (1995).

[69] U. Baur, F. Halzen, S. Keller, M.L. Mangano, and K. Riesselmann, Phys. Lett. B **318**, 544 (1993).

[70] M. Mangano, Nucl. Phys. **B405**, 536 (1993); P.J. Rijken and W.L. van Neerven, Phys. Rev. D **52**, 149 (1995).

[71] H. Baer, V. Barger, and R.J.N. Phillips, Phys. Rev. D **39**, 3310 (1989); *ibid.* **39**, 2809 (1989); R. Kleiss, A.D. Martin, and W.J. Stirling, Z. Phys. C **39**, 393 (1988); S. Gupta and D.P. Roy, *ibid.* **39**, 417 (1988).

[72] P. Nason, S. Dawson, and R.K. Ellis, Nucl. Phys. **B327**, 49 (1988); W. Beenakker *et al.*, *ibid.* **B351**, 507 (1991); E. Laenen, J. Smith, and W.L. van Neerven, *ibid.* **B369**, 543 (1992); Phys. Lett. **B321**, 254 (1994); M. Mangano, P. Nason, and G. Ridolfi, Nucl. Phys. **B373**, 295 (1992); S. Frixione *et al.*, Phys. Lett. B **351**, 555 (1995); N. Kidonakis and J. Smith, Phys. Rev. D **51**, 6092 (1995); E. Reya and P. Zerwas, in *Proceedings of the ECFA Workshop on LHC Physics* [60], Vol. II, p. 296.

[73] U. Baur and E.L. Berger, Phys. Rev. D **47**, 4889 (1993).

[74] G. Landsberg, in *Physics at Current Accelerators and Supercolliders*, Proceedings of the Workshop, Argonne, Illinois, 1993, edited by J.L. Hewett, A.R. White, and D. Zeppenfeld, p. 303.

[75] R. L. Sekulin, Phys. Lett. B **338**, 369 (1994).

[76] P. Mättig *et al.*, in *e^+e^- Collisions at 500 GeV: The Physics Potential*, Proceedings of the Workshop, Munich, Annecy, Hamburg, 1991, edited by P. Zerwas (DESY Report No. 92-123A, Namburg, 1992), p. 223; M. Bilenky *et al.*, Nucl. Phys. **B419**, 240 (1994); T. Barklow, in *Physics and Experiments with Linear Colliders*, Proceedings of the Workshop, Saariselka, Finland, 1991, edited by P. Orava, P. Eerola, and M. Nordberg, (World Scientific, Singapore, 1992), Vol. I, p. 423; T. Barklow, in *The Albuquerque Meeting* [14], p. 1236.

[77] S. Myers, Report No. CERN-SL-95-066, 1995 (unpublished) and talk given at the 2nd General Meeting of the LEP II Workshop, Report No. CERN, 1995 (unpublished).